Theory of the ground-state spin of the NV$^-$ center in diamond

M. W. Doherty,[1] F. Dolde,[2] H. Fedder,[2] F. Jelezko,[2,3] J. Wrachtrup,[2] N. B. Manson,[4] and L. C. L. Hollenberg[1]
[1]*School of Physics, University of Melbourne, Victoria 3010, Australia*
[2]*3rd Institute of Physics and Research Center SCOPE, University Stuttgart, Pfaffenwaldring 57, D-70550 Stuttgart, Germany*
[3]*Institut für Quantenoptik, Universität Ulm, Ulm D-89073, Germany*
[4]*Laser Physics Centre, Research School of Physics and Engineering, Australian National University, Australian Capital Territory 0200, Australia*
(Received 19 July 2011; published 3 May 2012)

The ground-state spin of the negatively charged nitrogen-vacancy center in diamond has been the platform for the recent rapid expansion of new frontiers in quantum metrology and solid-state quantum-information processing. However, in spite of its many outstanding demonstrations, the theory of the spin has not yet been fully developed, and there do not currently exist thorough explanations for many of its properties, such as the anisotropy of the electron g factor and the existence of Stark effects and strain splittings. In this work, the theory of the ground-state spin is fully developed using the molecular orbital theory of the center in order to provide detailed explanations for the spin's fine and hyperfine structures and its interactions with electric, magnetic, and strain fields. Given these explanations, a general solution is obtained for the spin in any given electric-magnetic-strain field configuration, and the effects of the fields on the spin's coherent evolution, relaxation, and inhomogeneous dephasing are examined. Thus, this work provides the essential theoretical tools for the precise control and modeling of this remarkable spin in its current and future applications.

DOI: 10.1103/PhysRevB.85.205203 PACS number(s): 71.70.Ej, 31.15.xh, 76.30.Mi

I. INTRODUCTION

The negatively charged nitrogen-vacancy (NV$^-$) center is a unique defect in diamond that has many promising applications in quantum metrology and quantum-information processing (QIP). In particular, the ground-state spin has been used in recent demonstrations of high-precision magnetic[1–11] and electric field[12] sensing, as well as spin-photon[13] and spin-spin[14–18] entanglement. The NV$^-$ center has also been employed to explore the developing decoherence-based sensing techniques.[19–22] Each of these demonstrations exploit the interaction of the spin with some configuration of electric, magnetic, and strain fields and the center's remarkable capability of optical spin polarization and readout.[23,24] The demonstration of electric field sensing,[12] which required the precise control of the spin using magnetic fields and the intricate modeling of the spin's interaction with electric, magnetic, and strain fields, highlighted the NV$^-$ center as a universal field sensor at the nanoscale as well as emphasized the requirement for a more detailed theoretical understanding of this important spin in diamond. The development of such an understanding will enable more precise control and modeling of the spin in its current applications and also provide the necessary insight to explore its future applications.

The NV$^-$ center is a point defect of C_{3v} symmetry in diamond consisting of a substitutional nitrogen atom adjacent to a carbon vacancy (refer to Fig. 1). The center's electronic structure is summarized in Fig. 2. It consists of a $^3A_2$ ground triplet state, an optical ^3E excited triplet, and several dark singlet states.[25] The fine structure of the ^3E excited triplet is highly dependent on temperature[26] and crystal strain,[27] whereas the fine structure of the $^3A_2$ ground triplet state is observed to be only weakly dependent on temperature[28] and crystal strain with a single zero-field splitting of $D_{gs} \sim 2.87$ GHz between the $m_s = 0$ and ± 1 spin sublevels. At ambient temperatures, the fine structure of the excited triplet state replicates the ground triplet state with a single zero-field splitting of $D_{es} \sim 1.42$ GHz,[29,30] independent of crystal strain due to the dynamic Jahn-Teller effect.[26] Zeeman and Stark splittings have been observed in the fine structures of both triplet states,[29,31–33] although the Stark effect in the ground triplet state is several orders of magnitude smaller than in the excited triplet state.[32,33]

One of the most intriguing properties of the NV$^-$ center is the ability to optically polarize and read out the ground-state spin,[23,24] distinguishing the center from other paramagnetic defects in diamond, and forming the basis for its QIP and quantum metrology applications. As depicted in Fig. 2, the process of optical spin polarization occurs due to the presence of a nonradiative decay pathway from the excited triplet state to the ground triplet state that competes with the optical decay pathway. The details of the photokinetics of the nonradiative pathway are yet to be fully explained, but it is believed that the $m_s = \pm 1$ sublevels of the excited triplet state are preferentially depopulated and the $m_s = 0$ sublevel of the ground triplet state is preferentially populated, thereby polarizing the population into the $m_s = 0$ spin state after optical cycling.[23,24] The preferential nonradiative depopulation of the $m_s = \pm 1$ sublevels of the excited triplet state also introduces a difference in the optical emission intensity between the spin sublevels. This difference in emission intensity can be utilized to read out the relative populations of the $m_s = 0$ and ± 1 sublevels of the ground triplet state through the measurement of the integrated emission intensity upon optical excitation.[23,24]

The center's capability of optical spin polarization and readout enables the implementation of continuous wave and pulsed optically detected magnetic resonance (ODMR) techniques.[23,24] Simple pulsed ODMR techniques such as free induction decay (FID) and spin echo[36,37] as well as more complicated multipulse ODMR techniques[6,38,39] have been implemented in the center's quantum metrology and

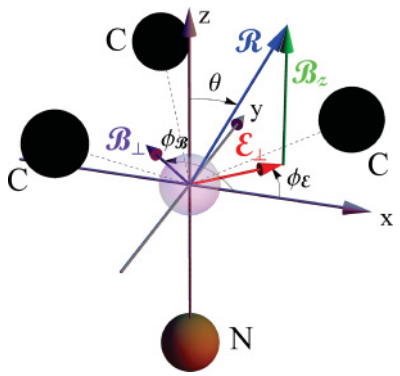

FIG. 1. (Color online) Schematic of the nitrogen-vacancy center and the adopted coordinate system, depicting the vacancy (transparent), the nearest-neighbor carbon atoms to the vacancy (black), the substitutional nitrogen atom (brown), the effective magnetic and electric-strain field components (colored arrows), and their corresponding field angles.

QIP applications and involve optical polarization and readout pulses encompassing a sequence of microwave pulses tuned to the fine-structure splittings of the ground triplet state. The microwave pulses coherently manipulate the ground-state spin and result in an optically detectable oscillation in the relative population of the $m_s = 0$ and ± 1 sublevels. In order to optimally control the spin and elicit the maximum amount of information and sensitivity from its implementation in ODMR experiments, a detailed model of the time evolution, relaxation, and dephasing of the spin is required.

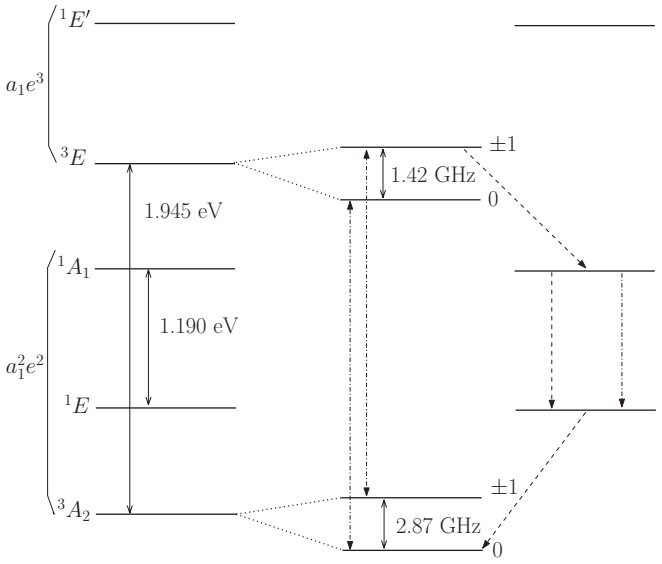

FIG. 2. The electronic orbital structure (left) and fine structure (right) at ambient temperatures formed from the ground $a_1^2e^2$ and first excited a_1e^3 molecular orbital configurations. The observed optical zero phonon line (1.945 eV) (Ref. 34) and infrared zero phonon line (1.190 eV) (Ref. 35) transitions are depicted as solid arrows in the orbital structure. The radiative (chain arrows) and nonradiative (dashed arrows) pathways that result in the optical spin polarization and readout of the center are depicted in the fine structure. Note that the much weaker radiative and nonradiative transitions that act to reduce spin polarization have not been depicted.

Electron spin resonance[40] (ESR) and *ab initio* studies[41–49] have confirmed that the electronic states of the center are highly localized to the vacancy and its nearest neighbors. The localization of the center's electronic states supports the application of a molecular model, in which the center's states are approximated by configurations of molecular orbitals (MOs). The molecular model has been successfully applied to describe the effects of electric, magnetic, and strain fields on the fine structure of the excited triplet state,[27,29,32] however, the model has not yet been applied to describe the effects of the fields on the ground triplet state. This has been due to an absence of the spin-orbit and spin-spin induced couplings of the center's electronic states, which have been obtained recently in Ref. 25. Consequently, until now, the measurements of the effects of the fields on the ground-state spin have been interpreted in terms of the canonical parameters of the effective spin-Hamiltonian formalism of ESR.[33,40,50,51] While the spin-Hamiltonian formalism has provided a practical model for the implementation of the center's applications, its canonical parameters alone do not facilitate the identification of their physical origins. A complementary first-principles treatment is required to derive expressions for the spin-Hamiltonian parameters and to correlate the properties of the ground-state spin to the other properties of the center. Furthermore, such a first-principles treatment enables the theoretical prediction of more intricate properties of the spin that may not have been identified in initial observations. The success of the molecular model in describing the properties of the excited triplet state motivates its implementation as the required first-principles treatment to understand the ground-state spin in greater detail.

In this article, the well-established molecular model[25,50,52,53] of the NV^- center will be applied in order to fully develop the theory of the ground-state spin. The fine and hyperfine structures and their corresponding eigenstates will be constructed prior to examining the effect of electric, magnetic, and strain fields on each. By using the matrix representations derived in the recently published electronic solution,[25] explicit expressions in terms of the center's MOs will be derived in this work for the hyperfine interaction with the ^{14}N nucleus, the components of the electron g-factor tensor, and the Stark and strain interactions. The derivation of these expressions enables the rigorous definition of the spin Hamiltonian of the ground-state spin and the correlation of the accurately measured parameters of the spin to the other observed properties of the center. The expressions will also assist future *ab initio* studies to independently calculate the properties of the ground-state spin.

The theory developed in Secs. II and III of this article will be applied in the subsequent sections in order to produce the solution of the ground-state spin and its time evolution in the presence of a general electric-magnetic-strain field configuration. The solution will be demonstrated by modeling a simple free induction decay experiment and examining the dependence of the FID signal, inhomogeneous dephasing, and spin relaxation on the applied field configuration. This simple demonstration will provide insight into the observed strong dependence of the spin's inhomogeneous dephasing time on the applied fields.[12] Furthermore, the spin solution will be a useful tool in future applications of the spin in quantum metrology and QIP as it clearly describes how electric,

magnetic, and strain fields can be used to precisely control this important spin in diamond, for example, multimodal decoherence microscopy that maps both magnetic and electric noise using the same probe.[19–22]

II. ELECTRONIC FINE STRUCTURE AND INTERACTIONS WITH ELECTRIC, MAGNETIC, AND STRAIN FIELDS

By adopting the adiabatic approximation and considering the nuclei of the crystal to be fixed at their equilibrium coordinates $\vec{R}_0$ corresponding to the ground electronic state, the electronic Hamiltonian $\hat{H}_e$ of the NV$^-$ center can be defined as

$$\hat{H}_e = \sum_i \hat{T}_i + \hat{V}_{Ne}(\vec{r}_i,\vec{R}_0) + \hat{V}_{so}(\mathbf{x}_i,\vec{R}_0) + \hat{V}_{hf}(\mathbf{x}_i,\mathbf{X}_0) + \sum_{i>j} \hat{V}_{ee}(\mathbf{x}_i,\mathbf{x}_j) + \hat{V}_{ss}(\mathbf{x}_i,\mathbf{x}_j), \quad (1)$$

where $\mathbf{x}_i = (\vec{r}_i,\vec{s}_i)$ denotes the collective spatial and spin coordinates of the ith electron of the center, $\mathbf{X}_0 = (\vec{R}_0,\vec{I})$ denotes the collective equilibrium spatial and spin coordinates of the crystal nuclei, $\hat{T}_i$ is the kinetic energy of the ith electron, $\hat{V}_{Ne}$ is the effective Coulomb potential of the interaction of the nuclei and lattice electrons with the electrons of the center, $\hat{V}_{so}$ is the electronic spin-orbit potential, $\hat{V}_{hf}$ is the hyperfine potential of the interactions between the crystal nuclei and the electrons of the center, $\hat{V}_{ee}$ is the Coulomb repulsion potential of the electrons of the center, and $\hat{V}_{ss}$ is the electronic spin-spin potential.

Ab initio studies[41–49] have confirmed the presence of three MOs (a_1, e_x, e_y) in the band gap of diamond and the center's observable electronic structure has been shown to consist of the ground $a_1^2e^2$ and first excited a_1e^3 MO configurations formed from the occupation of the MOs by four electrons.[25] Note that the other two electrons of the six electrons associated with the center occupy delocalized A_1 symmetric MOs within the diamond valence band and do not influence the observable properties of the center. The electronic states can be constructed by first defining orbital states with well-defined C_{3v} orbital symmetry formed from products of the MOs and defining spin states with well-defined C_{3v} spin symmetry.[25] Second, electronic states $\Phi^{so}_{n,j,k}$ that transform as specific rows k of irreducible representations j of the C_{3v} group in spin-orbit space are formed from linear combinations of the orbital and spin-state products.[25] Note that the quantum number n denotes the fine-structure level of the electronic state. For example, using the irreducible representations contained in Ref. 52, the electronic states of the ground triplet are

$$\begin{aligned}
\Phi^{so}_{1,A_1} &= \Phi_{A_2}S_{A_2} = \frac{1}{\sqrt{2}}(|a_1\bar{a}_1e_x\bar{e}_y\rangle + |a_1\bar{a}_1\bar{e}_xe_y\rangle),\\
\Phi^{so}_{2,E,x} &= -\Phi_{A_2}S_{E,y} = \frac{1}{\sqrt{2}}(|a_1\bar{a}_1e_xe_y\rangle - |a_1\bar{a}_1\bar{e}_x\bar{e}_y\rangle),\\
\Phi^{so}_{2,E,y} &= \Phi_{A_2}S_{E,x} = \frac{-i}{\sqrt{2}}(|a_1\bar{a}_1e_xe_y\rangle + |a_1\bar{a}_1\bar{e}_x\bar{e}_y\rangle),
\end{aligned} \quad (2)$$

where $\Phi_{A_2} = \frac{1}{\sqrt{2}}(a_1a_1e_xe_y - a_1a_1e_ye_x)$ is the A_2 orbital state of the ground triplet, the kets on the right-hand side denote Slater determinants (overbar denoting down spin), and the symmetrized $S = 1$ spin states in terms of the S_z eigenstates $\{|S,m_s\rangle\}$ are $S_{A_2} = |1,0\rangle$, $S_{E,x} = \frac{-i}{\sqrt{2}}(|1,1\rangle + |1,-1\rangle)$, and $S_{E,y} = \frac{-1}{\sqrt{2}}(|1,1\rangle - |1,-1\rangle)$.

The majority of the spin-orbit states $\Phi^{so}_{n,j,k}$ are eigenstates of the orbital components of the electronic Hamiltonian $\hat{H}_o = \sum_i \hat{T}_i + \hat{V}_{Ne}(\vec{r}_i,\vec{R}_0) + \sum_{i>j}\hat{V}_{ee}(\mathbf{x}_i,\mathbf{x}_j)$ with orbital energies denoted by $E_{J;S}$ (where, to remain consistent with Ref. 25, J denotes the irreducible representation of the orbital state and S denotes the total spin of the spin states used to form $\Phi^{so}_{n,j,k}$, and the orbital energy of the ground triplet is defined as $E_{A_2;1} = 0$). Only the spin-orbit states $(\Phi^{so}_{3,E,x},\Phi^{so}_{3,E,y},\Phi^{so}_{9,E,x},\Phi^{so}_{9,E,y})$ associated with the ^1E and $^1E'$ singlets are not eigenstates of $\hat{H}_o$ and are mixed by the Coulomb coupling coefficient κ (refer to Ref. 25 for further details). The energies $E_{J;S}$ including the effects of the Coulomb repulsion of the E singlets form the orbital structure of the center depicted in Fig. 2.

The electronic spin-orbit and spin-spin potentials can be treated as first-order perturbations to $\hat{H}_o$ using the orbital energies $E_{J;S}$ and the spin-orbit states $\Phi^{so}_{n,j,k}$ (accounting for Coulomb coupling) as the zero-order energies and states of the perturbation expansion. The perturbed energies correct to first order E_n have been shown to be consistent with the observed fine structure of the center depicted in Fig. 2.[27] It is found that the fine structure of the ground triplet state is governed by electronic spin-spin interaction, which splits the $m_s = 0$ and ±1 spin sublevels such that $E_2 - E_1 = D_{gs} \sim 2.87$ GHz, where

$$D_{gs} = \frac{3\mu_0 g_e^2\mu_B^2}{8\pi}\langle e_x(\vec{r}_1)e_y(\vec{r}_2)|\frac{1-3z_{12}^2/|\vec{r}_{12}|^2}{|\vec{r}_{12}|^3} \times [|e_x(\vec{r}_1)e_y(\vec{r}_2)\rangle - |e_y(\vec{r}_1)e_x(\vec{r}_2)\rangle], \quad (3)$$

μ_0 is the vacuum permeability, $g_e = 2.0023$ is the free electron g factor, μ_B is the Bohr magneton, $\vec{r}_i = x_i\vec{x} + y_i\vec{y} + z_i\vec{z}$ ($\vec{x},\vec{y},\vec{z}$ being unit coordinate vectors), $\vec{r}_{12} = \vec{r}_2 - \vec{r}_1$, and $z_{12} = z_2 - z_1$. As obtained in Ref. 25, the first-order-corrected spin-orbit states $\Phi^{so\prime}_{n,j,k}$ have the general form

$$\Phi^{so\prime}_{n,j,k} = N_n\left(\Phi^{so}_{n,j,k} + \sum_{m\neq n} s_{n,m}\Phi^{so}_{m,j,k}\right), \quad (4)$$

where N_n are normalization constants and $s_{n,m}$ are the first-order spin coupling coefficients. Using the results of Ref. 25, the first-order spin-orbit states of the ground triplet are

$$\begin{aligned}
\Phi^{so\prime}_{1,A_1} &= \Phi^{so}_{1,A_1} + s_{1,4}\Phi^{so}_{4,A_1} + s_{1,8}\Phi^{so}_{8,A_1},\\
\Phi^{so\prime}_{2,E,k} &= \Phi^{so}_{2,E,k} + s_{2,3}\Phi^{so}_{3,E,k} + s_{2,5}\Phi^{so}_{5,E,k} + s_{2,6}\Phi^{so}_{6,E,k} + s_{2,9}\Phi^{so}_{9,E,k},
\end{aligned} \quad (5)$$

where $k = x,y$ and the spin coupling coefficients of the ground triplet are contained in Table I and are functions of the orbital energies $E_{J;S}$, the axial $\lambda_\parallel = 5.3$ GHz (Ref. 27) and nonaxial $\lambda_\perp \sim$ GHz spin-orbit parameters, the spin-spin parameters $D_{1,E,1} \sim$ MHz and $D_{1,E,2} \sim$ MHz, the Coulomb coupling coefficient κ, and the spin-spin coupling coefficient of the excited triplet $\eta = 0.053$.[25]

Note that recent strain measurements of the infrared zero phonon line[54] (ZPL) have indicated that the Coulomb coupling coefficient is significant ($\kappa \sim 0.3$) and therefore must be retained to second order in the spin coupling coefficients. Furthermore, it should be noted that since the spin-orbit

TABLE I. The spin coupling coefficients of the ground triplet correct to first order in spin-orbit and spin-spin interactions. The Coulomb coupling coefficient κ, the spin-orbit parameters ($\lambda_\parallel$, $\lambda_\perp$), the spin-spin parameters ($D_{1,E,1}$,$D_{1,E,2}$), and the spin-spin coupling coefficient of the excited triplet η are as defined in Ref. 25. Note that $N_\kappa = (1+|\kappa|^2)^{-1/2}$.

$$s_{1,4} = -2i\,\frac{\lambda_\parallel}{E_{A_1;0}}$$
$$s_{1,8} = -\sqrt{2}\,\frac{\lambda_\perp + D_{1,E,2}}{E_{E;1}}$$
$$s_{2,3} = iN_\kappa\kappa\,\frac{\lambda_\perp}{E_{E;0}}$$
$$s_{2,5} = -\sqrt{2}\,\frac{D_{1,E,1}}{E_{E;1}} - \eta\,\frac{\lambda_\perp - D_{1,E,2}}{E_{E;1}}$$
$$s_{2,6} = \frac{\lambda_\perp - D_{1,E,2}}{E_{E;1}} - \sqrt{2}\eta\,\frac{D_{1,E,1}}{E_{E;1}}$$
$$s_{2,9} = -iN_\kappa\,\frac{\lambda_\perp}{E_{E';0}}$$

and spin-spin parameters are expected to be of the order of $\sim 10^{-9}$–10^{-6} eV (MHz-GHz) and the orbital energies are expected to be of the order of $\sim 10^{-2}$–10^{1} eV, the spin coupling coefficients are expected to be of the order of 10^{-4}–10^{-10}. The relative magnitudes of the different coefficients will become important in determining the leading-order terms that contribute to the interactions of the ground-state spin with electric, magnetic, and strain fields.

Given (5) and the zero-order orbital and spin operator matrix representations contained in Ref. 25, matrix representations of the ground triplet using the basis of first-order-corrected spin-orbit states $\{\Phi^{so\prime}_{1,A_1}, \Phi^{so\prime}_{2,E,x}, \Phi^{so\prime}_{2,E,y}\}$ can be constructed for general one-electron orbital tensor operators $\hat{O}_{p,q} = \sum_i \hat{O}_{p,q}(\vec{r}_i)$, which transform as the row q of the irreducible representation p of the C_{3v} group, and the total spin operator $\vec{S} = \sum_i \vec{s}_i$ (see Table II). The matrix representations are expressed in their most simplified form in terms of one-electron reduced matrix elements and the center's MOs. The one-electron matrix elements and the associated reduced matrix elements are related by the Wigner-Eckart theorem[55]

$$\langle \phi_{f,g}(\vec{r}_1)|\hat{O}_{p,q}(\vec{r}_1)|\phi_{j,k}(\vec{r}_1)\rangle = \begin{pmatrix} j & p & f \\ k & q & g \end{pmatrix}^* \langle \phi_f||\hat{O}_p||\phi_j\rangle, \tag{6}$$

where $\phi_{j,k}$ and $\phi_{f,g}$ are MOs of symmetry (j,k) and (f,g), respectively, and $(\ldots|\ldots)$ are the Clebsch-Gordon coefficients defined in Ref. 52. The detailed model of the interactions of the ground-state spin with electric, magnetic, and strain fields can thus be developed by applying the matrix representations of Table II to each interaction in turn. As a result, the interactions will be expressed in their most simplified form in terms of the spin coupling coefficients, the MOs, and the reduced matrix elements.

A. Interactions with magnetic fields

Defining $\vec{B}$ to be the applied magnetic field that is assumed to be approximately constant over the dimensions of the NV^- center, the interaction of the center's electrons with the magnetic field is described by the potential[56]

$$\hat{V}_{\rm mag} = \frac{\mu_B}{\hbar}\sum_i (\vec{l}_i + g_e\vec{s}_i)\cdot\vec{B} + \frac{1}{2m_e c^2}[\vec{s}_i \times \vec{\nabla}\hat{V}_{Ne}(\vec{r}_i)]\cdot(\vec{B}\times\vec{r}_i), \tag{7}$$

where $\vec{l} = l_x\vec{x} + l_y\vec{y} + l_z\vec{z} = \vec{r}\times\vec{p}$ is the electron orbital magnetic moment, $\vec{p}$ is the electron momentum, $\hbar$ is the reduced Planck constant, m_e is the mass of an electron, and c is the speed of light. Note that the origin of the coordinate system is defined to be at the center of the NV^- defect, in the vicinity of the vacancy (as depicted in Fig. 1). Additionally, note that the term $\sum_i \frac{e^2}{8m_e}(\vec{B}\times\vec{r}_i)^2$ (where e is the electronic charge) quadratic in the magnetic field[56] has been neglected in the above definition since it does not induce a relative shift of the fine-structure levels or couple the electronic states of the ground triplet at first order in the spin coupling coefficients.

TABLE II. Matrix representations of the components of the total spin operator $\vec{S} = \sum_i \vec{s}_i$ and the orbital tensor operators $\hat{O}_{p,q} = \sum_i \hat{O}_{p,q}(\vec{r}_i)$ of different symmetry (p,q) correct to first order in the spin coupling coefficients in the basis of the corrected spin-orbit states $\{\Phi^{so\prime}_{1,A_1}, \Phi^{so\prime}_{2,E,x}, \Phi^{so\prime}_{2,E,y}\}$ of the ground triplet. The orbital parameters in terms of reduced matrix elements of the center's molecular orbitals are $o_{a,A_1} = 2(\langle a_1||\hat{O}_{A_1}||a_1\rangle + \langle e||\hat{O}_{A_1}||e\rangle)$ and $o_{a,E} = \langle a_1||\hat{O}_{A_1}||e\rangle$.

$$S_x = \begin{pmatrix} 0 & 0 & -i\hbar \\ 0 & 0 & 0 \\ i\hbar & 0 & 0 \end{pmatrix},\ S_y = \begin{pmatrix} 0 & i\hbar & 0 \\ -i\hbar & 0 & 0 \\ 0 & 0 & 0 \end{pmatrix},\ S_z = \begin{pmatrix} 0 & 0 & 0 \\ 0 & 0 & -i\hbar \\ 0 & i\hbar & 0 \end{pmatrix}$$

$$\hat{O}_{A_1} = \begin{pmatrix} o_{a,A_1} & 0 & 0 \\ 0 & o_{a,A_1} & 0 \\ 0 & 0 & o_{a,A_1} \end{pmatrix},\ \hat{O}_{A_2} = \begin{pmatrix} 0 & 0 & 0 \\ 0 & 0 & 0 \\ 0 & 0 & 0 \end{pmatrix}$$

$$\hat{O}_{E,x} = \begin{pmatrix} 0 & s_{2,6}o_{a,E} + \frac{s_{1,8}}{\sqrt{2}}o^*_{a,E} & 0 \\ s_{2,6}o^*_{a,E} + \frac{s_{1,8}}{\sqrt{2}}o_{a,E} & -\frac{1}{\sqrt{2}}s_{2,5}(o_{a,E} + o^*_{a,E}) & 0 \\ 0 & 0 & \frac{1}{\sqrt{2}}s_{2,5}(o_{a,E} + o^*_{a,E}) \end{pmatrix}$$

$$\hat{O}_{E,y} = \begin{pmatrix} 0 & 0 & s_{2,6}o_{a,E} + \frac{s_{1,8}}{\sqrt{2}}o^*_{a,E} \\ 0 & 0 & \frac{1}{\sqrt{2}}s_{2,5}(o_{a,E} + o^*_{a,E}) \\ s_{2,6}o^*_{a,E} + \frac{s_{1,8}}{\sqrt{2}}o_{a,E} & \frac{1}{\sqrt{2}}s_{2,5}(o_{a,E} + o^*_{a,E}) & 0 \end{pmatrix}$$

TABLE III. Experimental measurements and *ab initio* calculations of the effective g factor and hyperfine parameters of the NV$^-$ center tabulated by reference.

Ref.	$g_\perp$	$g_\parallel$	$A_\perp/h$ (MHz)	$A_\parallel/h$ (MHz)	P/h (MHz)
Loubser (Ref. 50) (Expt.)	2.0028 ± 0.0003	2.0028 ± 0.0003		$(\pm)2.32 \pm 0.01$	
He (Ref. 40) (Expt.)	2.0028 ± 0.0003	2.0028 ± 0.0003	$(+)2.10 \pm 0.10$	$(+)2.30 \pm 0.02$	$(-)5.04 \pm 0.05$
Felton (Ref. 51) (Expt.)	2.0031 ± 0.0002	2.0029 ± 0.0002	$(-)2.70 \pm 0.07$	$(-)2.14 \pm 0.07$	$(-)5.01 \pm 0.06$
Steiner (Ref. 57) (Expt.)				-2.166 ± 0.01	-4.945 ± 0.01
Smeltzer (Ref. 58) (Expt.)				-2.162 ± 0.002	-4.945 ± 0.005
Gali (Ref. 49) (*Ab initio*)			$(-)1.7$	$(-)1.7$	

The second term in (7) arises from relativistic corrections to the nonrelativistic first term[56] and can be written in the more explicit form

$$\frac{1}{2m_e c^2}(\vec{s} \times \vec{\nabla}\hat{V}_{Ne}) \cdot (\vec{B} \times \vec{r}) = \frac{1}{2m_e c^2}\vec{s} \cdot \bar{G} \cdot \vec{B}, \tag{8}$$

where the orbital operator $\bar{G}$ is the matrix

$$\begin{pmatrix} \frac{\partial \hat{V}_{Ne}}{\partial y}y + \frac{\partial \hat{V}_{Ne}}{\partial z}z & -\frac{\partial \hat{V}_{Ne}}{\partial y}x & -\frac{\partial \hat{V}_{Ne}}{\partial z}x \\ -\frac{\partial \hat{V}_{Ne}}{\partial x}y & \frac{\partial \hat{V}_{Ne}}{\partial x}x + \frac{\partial \hat{V}_{Ne}}{\partial z}z & -\frac{\partial \hat{V}_{Ne}}{\partial z}y \\ -\frac{\partial \hat{V}_{Ne}}{\partial x}z & -\frac{\partial \hat{V}_{Ne}}{\partial y}z & \frac{\partial \hat{V}_{Ne}}{\partial x}x + \frac{\partial \hat{V}_{Ne}}{\partial y}y \end{pmatrix}.$$

The tensor components of the orbital operators contained in (7), as obtained from the definitions of $\vec{l}$ and $\bar{G}$ and the C_{3v} representations defined in Ref. 52, are

$$\begin{aligned} l_{E,x} &= l_y,\ l_{E,y} = -l_x,\ l_{A_2} = l_z, \\ G_{1,A_1} &= \frac{\partial \hat{V}_{Ne}}{\partial x}x + \frac{\partial \hat{V}_{Ne}}{\partial y}y,\ G_{2,A_1} = \frac{\partial \hat{V}_{Ne}}{\partial z}z, \\ G_{1,E,x} &= \frac{\partial \hat{V}_{Ne}}{\partial x}x - \frac{\partial \hat{V}_{Ne}}{\partial y}y,\ G_{2,E,x} = \frac{\partial \hat{V}_{Ne}}{\partial z}x, \\ G_{3,E,x} &= \frac{\partial \hat{V}_{Ne}}{\partial x}z,\ G_{1,E,y} = -\frac{\partial \hat{V}_{Ne}}{\partial x}y - \frac{\partial \hat{V}_{Ne}}{\partial y}x, \\ G_{2,E,y} &= \frac{\partial \hat{V}_{Ne}}{\partial z}y,\ G_{3,E,y} = \frac{\partial \hat{V}_{Ne}}{\partial y}z. \end{aligned} \tag{9}$$

Hence, using the general matrix representations of Table II, the matrix representation of the magnetic interaction (7) with the ground triplet can be obtained correct to first order in the spin coupling coefficients

$$V_{\text{mag}} = \mu_B \begin{pmatrix} 0 & ig_\perp B_y & -ig_\perp B_x \\ -ig_\perp B_y & 0 & -ig_\parallel B_z \\ ig_\perp B_x & ig_\parallel B_z & 0 \end{pmatrix}, \tag{10}$$

where

$$\begin{aligned} g_\perp &= g_e + \left(s_{2,6} - \frac{s_{1,8}}{\sqrt{2}}\right)l_{a,E} + \frac{1}{2}g_{1,A_1} + g_{2,A_1}, \\ g_\parallel &= g_e + g_{1,A_1}, \end{aligned} \tag{11}$$

and $l_{a,E} = -i\langle a_1||l_E||e\rangle/\sqrt{2}\hbar$, $g_{1,A_1} = \langle e||G_{1,A_1}||e\rangle/2m_e c^2$, and $g_{2,A_1} = \langle e||G_{2,A_1}||e\rangle/2m_e c^2$. Given that the relativistic term (8) is much smaller than the nonrelativistic term, only contributions of the relativistic term that are zero order in the spin coupling coefficients have been included.

Comparing (10) with the matrix representations of the total spin operators in Table II, it can be seen that the magnetic interaction can be written in the spin-Hamiltonian form $\hat{V}_{\text{mag}} = \frac{\mu_B}{\hbar}\vec{S} \cdot \bar{g} \cdot \vec{B}$, where the effective g-factor tensor $\bar{g}$ is defined as

$$\bar{g} = \begin{pmatrix} g_\perp & 0 & 0 \\ 0 & g_\perp & 0 \\ 0 & 0 & g_\parallel \end{pmatrix}. \tag{12}$$

The parameters $g_\perp$ and $g_\parallel$ may then be identified as the nonaxial and axial effective g-factor components, respectively. The g-factor components have been measured by several ESR studies,[40,50,51] and the observed values are contained in Table III. The measurements conclusively show that both $g_\parallel$ and $g_\perp$ are shifted by $+6 \pm 1 \times 10^{-4}$ from the free-electron g factor $g_e = 2.0023$, and one study[51] observed a small anisotropy of $g_\perp - g_\parallel = 2 \times 10^{-4}$. From (11) it is clear that there is no orbital magnetic moment contribution to $g_\parallel$ at first order in the spin coupling coefficients, and due to the expected orders of magnitudes of the coefficients, any second-order contribution would be much smaller than the observed shifts of $g_\parallel$ and $g_\perp$. Thus, only the relativistic term (8), which shifts $g_\parallel$ from g_e by the addition of g_{1,A_1} and also shifts $g_\perp$ by the addition of $\frac{1}{2}g_{1,A_1} + g_{2,A_1}$ can explain the observed shifts. The different contributions of the relativistic term to $g_\perp$ and $g_\parallel$ can also explain the small anisotropy; however, if the orbital magnetic moment contribution to $g_\perp$ is large enough, it may also contribute at the same order as the relativistic term. The leading-order term of the orbital magnetic moment contribution to $g_\perp$ is

$$\left(s_{2,6} - \frac{s_{1,8}}{\sqrt{2}}\right)l_{a,E} \approx 2\frac{\lambda_\perp}{E_{E;1}}l_{a,E} \tag{13}$$

due to the expectation that $\lambda_\perp \gg \eta D_{1,E,2}$. Through the observation of the magnetic circular dichroism (MCD) of the optical ZPL,[26] the orbital magnetic moment parameter will be of the order $l_{a,E} \sim 10^{-1}$. Consequently, the orbital magnetic moment will only contribute significantly to the g-factor anisotropy if $2\frac{\lambda_\perp}{E_{E;1}} \sim 10^{-3}$, which given $E_{E;1} \approx 2.180$ eV (Ref. 25) implies that $\lambda_\perp$ would have to be of the order of 1 meV $\sim$ 1 THz, a dramatic difference from the axial spin-orbit parameter $\lambda_\parallel = 5.3$ GHz. Such a dramatic difference is improbable given the NV$^-$ center's small departure from the higher T_d symmetry, in which the axial and nonaxial spin-orbit parameters are equal. Therefore, it appears unlikely that the orbital magnetic moment contributes significantly to $\bar{g}$.

B. Interactions with electric fields

Defining $\vec{E}$ to be the applied electric field that is assumed to be approximately constant over the dimensions of the NV^- center, the interaction of the center's electrons with the electric field is described by the potential[59]

$$\hat{V}_{\rm el} = \sum_i \vec{d}_i \cdot \vec{E}, \tag{14}$$

where $\vec{d} = e\vec{r}$ is the electron electric dipole moment. The tensor components of $\vec{d}$ are simply $\vec{d} = d_{E,x}\vec{x} + d_{E,y}\vec{y} + d_{A_1}\vec{z}$, and the ground triplet matrix representation of $\hat{V}_{el}$ correct to first order in the spin coupling coefficients is

$$V_{\rm el} = \begin{pmatrix} d_{a,A_1}E_z & d'_\perp E_x & d'_\perp E_y \\ d'_\perp E_x & d_{a,A_1}E_z + d_\perp E_x & -d_\perp E_y \\ d'_\perp E_y & -d_\perp E_y & d_{a,A_1}E_z - d_\perp E_x \end{pmatrix}, \tag{15}$$

where $d_{a,A_1} = 2(\langle a_1||d_{A_1}||a_1\rangle + \langle e||d_{A_1}||e\rangle)$, $d_\perp = -2s_{2,5}d_{a,E}$, $d'_\perp = (s_{2,6} + \frac{s_{1,8}}{\sqrt{2}})d_{a,E}$, and $d_{a,E} = \frac{1}{\sqrt{2}}\langle a_1||d_E||e\rangle$.

The leading-order terms of the two nonaxial dipole parameters are

$$d_\perp \approx 2\frac{\eta\lambda_\perp}{E_{E;1}}d_{a,E},\ d'_\perp \approx -2\frac{D_{1,E,2}}{E_{E;1}}d_{a,E}, \tag{16}$$

which, due to the potentially similar orders of magnitude of the numerators in each, suggests that the parameters are potentially of the same magnitude. However, since $d'_\perp$ couples electronic states separated in energy by D_{gs}, it can be ignored for static electric fields that satisfy $d'_\perp E_\perp \ll D_{gs}$, where $E_\perp = \sqrt{E_x^2 + E_y^2}$ is the nonaxial electric field strength. This conclusion is in agreement with observation,[12,33] where small linear Stark splittings of the $m_s = \pm 1$ fine-structure levels have been shown to agree with $d'_\perp \approx 0$ and $d_\perp/h = 17 \pm 3$ Hz cm/V.[33]

Since correct to first order in the spin coupling coefficients, the term $d_{a,A_1}E_z$ is common to each of the diagonal matrix elements, it appears that an axial electric field does not induce a relative shift of the fine-structure levels of the ground triplet. However, this conclusion is in conflict with observation,[33] where a very small linear shift of the zero-field splitting between the $m_s = 0$ and ± 1 fine-structure levels was observed and could be described only by a difference of $d_\parallel/h = 0.35 \pm 0.02$ Hz cm/V in the axial dipole parameters of the $m_s = 0$ and ± 1 spin-orbit states. Such a difference occurs at second order in the spin coupling coefficients, where the matrix representation of the interaction of the ground triplet with an axial electric field becomes

$$d_{A_1}E_z = \begin{pmatrix} d_{a,A_1}E_z & 0 & 0 \\ 0 & (d_{a,A_1} + d_\parallel)E_z & 0 \\ 0 & 0 & (d_{a,A_1} + d_\parallel)E_z \end{pmatrix}, \tag{17}$$

where $d_\parallel = (s_{2,5}^2 + s_{2,6}^2 + s_{2,9}^2)d_{b,A_1}$ and $d_{b,A_1} = \langle e||d_{A_1}||e\rangle - \langle a_1||d_{A_1}||a_1\rangle$. Therefore, the effective matrix representation of the interaction of the ground triplet with a static electric field satisfying $d'_\perp E_\perp \ll D_{gs}$ is

$$V_{\rm el} = \begin{pmatrix} 0 & 0 & 0 \\ 0 & d_\parallel E_z + d_\perp E_x & -d_\perp E_y \\ 0 & -d_\perp E_y & d_\parallel E_z - d_\perp E_x \end{pmatrix}. \tag{18}$$

This effective representation can be expressed in the spin-Hamiltonian form $\hat{V}_{\rm el} = \frac{1}{\hbar^2}d_\parallel E_z S_z^2 - \frac{1}{\hbar^2}d_\perp E_x(S_x^2 - S_y^2) + \frac{1}{\hbar^2}d_\perp E_y(S_xS_y + S_yS_x)$ used to describe the linear Stark effect present in C_{3v} symmetric systems in ESR.[60]

The dipole reduced matrix element $d_{a,E}$ contained in $d_\perp$ is also responsible for the center's optical transition,[25] and an estimate of its magnitude can be obtained from the center's observed radiative lifetime $T_R \approx 13$ ns,[61] using[62]

$$d_{a,E}/h = \left(\frac{6\pi\epsilon_0\hbar^4c^3}{\langle E_O^3\rangle n_D T_R}\right)^{\frac{1}{2}} \Big/ h, \tag{19}$$

where $\langle E_O^3\rangle = \int_0^\infty F(E_O)E_O^3 dE_O$ is the expectation value of the cube of the optical emission energy given the normalized vibrational sideband distribution $F(E_O)$,[63] and $n_D = 2.418$ is the refractive index of diamond. As the vibrational sideband of the center's optical emission extends from approximately 1.4 eV to the ZPL at 1.945 eV, the estimate of the dipole reduced matrix element is bounded by $3.65 \leqslant d_{a,E}/h \leqslant 5.98$ MHz cm/V [compare with, for example, the 5.41 MHz cm/V dipole moment of the $5s(^2S_{1/2}) \longleftrightarrow 5p(^2P_{3/2})$ transition of ^{87}Rb].[64]

The observed value of $d_\perp/h = 17 \pm 3$ Hz cm/V, [33] the estimated range of $d_{a,E}$, the approximate expression for $d_\perp \approx 2\frac{\eta\lambda_\perp}{E_{E;1}}d_{a,E}$, and $\eta = 0.053$ (Ref. 25) imply that $\frac{\lambda_\perp}{E_{E;1}} \sim 10^{-4}$ as expected, thereby supporting the assertion made in the previous section that the orbital magnetic moment does not contribute significantly to $\bar{g}$. The dipole reduced matrix element d_{b,A_1} contained in $d_\parallel$ also contributes to the shift of the center's optical ZPL in the presence of an axial electric field.[25] However, since the optical transition involves a change in MO configuration and, thus a change in the nuclear equilibrium coordinates,[25] both the axial electric and nuclear dipole moments contribute to the shift of the center's optical ZPL. Consequently, without knowledge of the nuclear dipole moment, it is not possible to estimate d_{b,A_1} given just measurements of the shift.

C. Interactions with strain fields

The interaction of the center's electrons with a crystal strain field can be approximately described by performing a Taylor series expansion of the electronic Hamiltonian $\hat{H}_e$ in terms of the displacements of the nuclear coordinates $\vec{R}$ from their ground-state equilibrium coordinates $\vec{R}_0$ induced by the strain field and retaining only the linear terms of the expansion. Defining $Q_{u,p,q}$ to be the uth normal nuclear displacement coordinate of the crystal that transforms as the row q of the irreducible representation p of the C_{3v} group, the strain potential is[62]

$$\hat{V}_{\rm str} = \sum_i \sum_{u,p,q} \left.\frac{\partial \hat{V}_{Ne}(\vec{r}_i, \vec{R})}{\partial Q_{u,p,q}}\right|_{\vec{R}_0} \xi_{u,p,q}, \tag{20}$$

where $\xi_{u,p,q}$ is the crystal strain along the displacement coordinate $Q_{u,p,q}$. Given that by definition $\partial \hat{V}_{Ne}(\vec{r}_i,\vec{R})/\partial Q_{u,p,q}|_{\vec{R}_0}$ is an orbital tensor operator of symmetry (p,q), the ground triplet matrix representation of $\hat{V}_{\rm str}$ is analogous to that of $\hat{V}_{\rm el}$. Treating the nonaxial terms correct to first order and the axial terms correct to second order in the spin coupling coefficients, the matrix representation of $\hat{V}_{\rm str}$ is

$$V_{\rm str} = \begin{pmatrix} \zeta'_z & \zeta'_x & \zeta'_y \\ \zeta'_x & \zeta'_z+\zeta_z+\zeta_x & -\zeta_y \\ \zeta'_y & -\zeta_y & \zeta'_z+\zeta_z-\zeta_x \end{pmatrix}, \tag{21}$$

where

$$\begin{aligned}
\zeta'_z &= \sum_u \zeta_{u,a,A_1}\xi_{u,A_1},\\
\zeta_z &= \left(s^2_{2,5}+s^2_{2,6}+s^2_{2,9}\right)\sum_u \zeta_{u,b,A_1}\xi_{u,A_1},\\
\zeta'_k &= \left(s_{2,6}+\frac{s_{1,8}}{\sqrt{2}}\right)\sum_u \zeta_{u,a,E}\xi_{u,E,k},\\
\zeta_k &= -2s_{2,5}\sum_u \zeta_{u,a,E}\xi_{u,E,k},
\end{aligned} \tag{22}$$

$$\begin{aligned}
\zeta_{u,a,A_1} &= 2\langle a_1||\frac{\partial \hat{V}_{Ne}}{\partial Q_{u,A_1}}\Big|_{\vec{R}_0}||a_1\rangle + 2\langle e||\frac{\partial \hat{V}_{Ne}}{\partial Q_{u,A_1}}\Big|_{\vec{R}_0}||e\rangle,\\
\zeta_{u,b,A_1} &= \langle e||\frac{\partial \hat{V}_{Ne}}{\partial Q_{u,A_1}}\Big|_{\vec{R}_0}||e\rangle - \langle a_1||\frac{\partial \hat{V}_{Ne}}{\partial Q_{u,A_1}}\Big|_{\vec{R}_0}||a_1\rangle,\\
\zeta_{u,a,E} &= \frac{1}{\sqrt{2}}\langle a_1||\frac{\partial \hat{V}_{Ne}}{\partial Q_{u,E}}\Big|_{\vec{R}_0}||e\rangle,
\end{aligned}$$

and $k = x, y$. Note that torsional strain components that have displacement coordinates that transform as A_2 have been ignored.

Similar to $\hat{V}_{\rm el}$, the diagonal contributions ζ'_z do not shift the fine-structure levels of the ground triplet with respect to each other and thus can be effectively ignored. Likewise, for nonaxial strains that satisfy $\zeta'_\perp \ll D_{gs}$ (where $\zeta'_\perp = \sqrt{\zeta'^2_x+\zeta'^2_y}$), ζ'_x and ζ'_y will have negligible effect on the fine-structure levels and state coupling and thus can also be ignored. Defining the effective strain field $\vec{\sigma} = \sigma_x\vec{x}+\sigma_y\vec{y}+\sigma_z\vec{z} = \zeta_x/d_\perp\vec{x} + \zeta_y/d_\perp\vec{y}+\zeta_z/d_\parallel\vec{z}$, the effective matrix representation of $\hat{V}_{\rm str}$ becomes

$$V_{\rm str} = \begin{pmatrix} 0 & 0 & 0 \\ 0 & d_\parallel\sigma_z+d_\perp\sigma_x & -d_\perp\sigma_y \\ 0 & -d_\perp\sigma_y & d_\parallel\sigma_z-d_\perp\sigma_x \end{pmatrix} \tag{23}$$

and it is clear that the strain field can be treated as an additional effective local electric field $\vec{\sigma}$ at the center. Hence, by defining the total effective electric field $\vec{\Pi} = \vec{E}+\vec{\sigma}$, the interaction of the center with both strain and electric fields can be expressed in the spin-Hamiltonian form $\hat{V}_{\rm el}+\hat{V}_{\rm str} = \frac{1}{\hbar^2}d_\parallel\Pi_z S_z^2 - \frac{1}{\hbar^2}d_\perp\Pi_x(S_x^2-S_y^2)+\frac{1}{\hbar^2}d_\perp\Pi_y(S_xS_y+S_yS_x)$.

D. Complete spin Hamiltonian

Including the descriptions of the spin-spin zero-field splitting and interactions with magnetic, electric, and strain fields obtained in the previous sections, the complete electronic spin-Hamiltonian of the ground-state spin becomes

$$\begin{aligned}
\hat{H}_{gs} = &\frac{1}{\hbar^2}(D_{gs}+d_\parallel\Pi_z)S_z^2 + \frac{\mu_B}{\hbar}\vec{S}\cdot\bar{g}\cdot\vec{B}\\
&-\frac{1}{\hbar^2}d_\perp\Pi_x\left(S_x^2-S_y^2\right)+\frac{1}{\hbar^2}d_\perp\Pi_y(S_xS_y+S_yS_x),
\end{aligned} \tag{24}$$

which in the spin basis $\{S_{A_2}, -S_{E,y}, S_{E,x}\}$ associated with the ground triplet spin-orbit states has the matrix representation

$$\hat{H}_{gs} = \begin{pmatrix} 0 & i\mathcal{B}_y & -i\mathcal{B}_x \\ -i\mathcal{B}_y & \mathcal{D}+\mathcal{E}_x & -i\mathcal{B}_z-\mathcal{E}_y \\ i\mathcal{B}_x & i\mathcal{B}_z-\mathcal{E}_y & \mathcal{D}-\mathcal{E}_x \end{pmatrix}, \tag{25}$$

where $\mathcal{D} = D_{gs}+d_\parallel\Pi_z$, $\mathcal{B}_z = \mu_B g_\parallel B_z$, $\mathcal{E}_k = d_\perp\Pi_k$, $\mathcal{B}_k = \mu_B g_\perp B_k$, and $k = x,y$. This final matrix representation provides the simplest description of the dependence of the ground-state spin on the six independent electric-magnetic-strain field parameters $(\mathcal{D},\mathcal{E}_x,\mathcal{E}_y,\vec{\mathcal{B}})$ and will be used to obtain the spin solution in Sec. IV.

III. NUCLEAR HYPERFINE STRUCTURE

The nuclear hyperfine interaction $\hat{V}_{hf} = \hat{V}_{mhf}+\hat{V}_{ehf}$ between the center's electrons and the nuclei of the crystal lattice has magnetic $\hat{V}_{mhf}$ and electric $\hat{V}_{ehf}$ components. The magnetic hyperfine component accounts for the interactions of the electronic spin and orbital magnetic moment with the nuclear spins of the lattice. Since it was found in the previous section that the ground triplet has no orbital magnetic moment at zero order in the spin coupling coefficients, the interaction between the orbital magnetic moment and the nuclear spins may be ignored. The electric hyperfine component approximately accounts for the finite size of the nuclei through the interaction of the center's electrons with the electric quadrupole moments of the finite charge distributions of the nuclei. The nuclei contained in a typical NV$^-$ diamond crystal include ^{12}C and the ^{14}N of the NV$^-$ center, as well as ^{13}C isotopic impurities and ^{14}N within other lattice defects. As ^{12}C has zero nuclear spin and thus also does not possess an electric quadrupole moment (only nuclei with spin $I \geqslant 1$ may possess electric quadrupole moments),[62] the ^{12}C nuclei do not contribute the nuclear hyperfine interaction of the NV$^-$ center. The ^{14}N nuclei of the center and other lattice defects do, however, contribute to both components of the nuclear hyperfine interaction as they possess both spin $I = 1$ and an electric quadrupole moment. The ^{13}C isotopic impurities only contribute to the magnetic hyperfine interaction since they have spin $I = 1/2$. In this section, only the internal hyperfine interactions between the NV$^-$ electrons and the NV$^-$ ^{14}N nucleus will be considered. Although, the extrinsic hyperfine interactions between the NV$^-$ center and the nuclear impurities of the crystal are significant, they will be ignored here due to their inherent sample dependence. The internal magnetic and electric hyperfine interactions of the NV$^-$ center are described

by the potentials[62]

$$\begin{aligned}\hat{V}_{mhf} &= C_{mhf}\sum_i\left(4\pi\delta(\vec{r}_{iN})-\frac{1}{|\vec{r}_{iN}|^3}\right)\vec{s}_i\cdot\vec{I}\\&\quad+\frac{3(\vec{s}_i\cdot\vec{r}_{iN})(\vec{r}_{iN}\cdot\vec{I})}{|\vec{r}_{iN}|^5},\\\hat{V}_{ehf} &= \frac{1}{2Z_N}\sum_{\alpha,a,b}\left(\sum_i\frac{\partial^2\hat{V}_e(\vec{r}_i)}{\partial R_{N,a}\partial R_{N,b}}\bigg|_{\vec{R}_0}\right.\\&\quad\left.+\frac{\partial^2 V_l}{\partial R_{N,a}\partial R_{N,b}}\bigg|_{\vec{R}_0}\right)u_{\alpha,a}u_{\alpha,b},\end{aligned}\tag{26}$$

where $C_{mhf}=\mu_B\mu_N g_e g_N\frac{\mu_0}{4\pi\hbar^2}$, μ_N is the nuclear magneton, $g_N=0.403\,56$ is the ^{14}N nuclear g factor,[59] $\vec{I}$ is the spin operator of the ^{14}N nucleus, $\vec{r}_{iN}=\vec{R}_N-\vec{r}_i=x_{iN}\vec{x}+y_{iN}\vec{y}+z_{iN}\vec{z}$, $\vec{R}_N=R_{N,x}\vec{x}+R_{N,y}\vec{y}+R_{N,z}\vec{z}$ is the position of the ^{14}N nucleus, $\hat{V}_e$ is the Coulomb interaction potential of the center's electrons with the ^{14}N nucleus, V_l is the Coulomb interaction potential of the lattice electrons and ^{12}C nuclei with the ^{14}N nucleus, $Z_N=7$ is the relative charge of the ^{14}N nucleus, and $u_{\alpha,a}$ and $u_{\alpha,b}$ are the components of the displacement of the αth ^{14}N proton from $\vec{R}_N$ in the $a,b=x,y,z$ directions.

The magnetic hyperfine interaction can be written as a sum of terms containing rank-two orbital tensor operators $\hat{V}_{mhf}=\sum_i\vec{s}_i\cdot[\bar{A}_{A_1}(\vec{r_{iN}})+\bar{A}_{E,x}(\vec{r_{iN}})+\bar{A}_{E,y}(\vec{r_{iN}})]\cdot\vec{I}$. By applying the matrix representations of Table II, it is clear that only the term containing $\bar{A}_{A_1}(\vec{r_{iN}})$ contributes at zero order in the spin coupling coefficients. Given this result, $\hat{V}_{mhf}$ can be written in the spin-Hamiltonian form $\hat{V}_{mhf}=\vec{S}\cdot\bar{A}\cdot\vec{I}$, where

$$\bar{A}=\begin{pmatrix}A_\perp & 0 & 0\\0 & A_\perp & 0\\0 & 0 & A_\parallel\end{pmatrix},$$

$A_\parallel=f_{A_1}+2a_{A_1}$ is the axial magnetic hyperfine parameter, $A_\perp=f_{A_1}-a_{A_1}$ is the nonaxial magnetic hyperfine parameter, $f_{A_1}=C_{mhf}4\pi\langle e||\delta(\vec{r}_{iN})||e\rangle$ is the Fermi contact contribution, and $a_{A_1}=\frac{1}{2}C_{mhf}\langle e||\frac{1}{|r_{iN}|^3}(\frac{3z_{iN}^2}{|\vec{r}_{iN}|^2}-1)||e\rangle$ is the dipolar contribution. Measured values of the magnetic hyperfine parameters are contained in Table III and, although they differ in sign and magnitude, conclusively show that both the Fermi contact and dipolar contributions must be nonzero. For example, using the values obtained in Ref. 51, $f_{A_1}/h=-2.51$ MHz and $a_{A_1}/h=187$ kHz.

The expression for the Fermi contact contribution can be simplified further to $f_{A_1}=C_{mhf}4\pi|e_x(\vec{R}_N)|^2=C_{mhf}4\pi|e_y(\vec{R}_N)|^2$. As the e MOs transform as the E irreducible representation of the C_{3v} group, they are by definition zero at any point along the axial symmetry axis of the center, and since the equilibrium position of the ^{14}N nucleus is on the axial symmetry axis, the Fermi contact contribution vanishes if the ^{14}N is fixed at its equilibrium position. To account for the nonzero Fermi contact contribution in the molecular model, the vibrational wave function $\chi_N(\vec{R}_N)$ of the ^{14}N must be considered, in which case the expression for the Fermi contact contribution becomes

$$f_{\text{vib}}=C_{mhf}4\pi\int|e_x(\vec{R}_N)|^2|\chi_N(\vec{R}_N)|^2d^3R_N.\tag{27}$$

A similar vibrationally corrected expression for the dipolar contribution can also be defined.

The magnetic polarization of the ^{14}N core electrons associated with the $m_s=\pm1$ states of the center will provide a negative Fermi contact contribution f_{core} (Refs. 49 and 51) in addition to the positive contribution arising from the vibrational motion of the nucleus. However, the description of f_{core} is beyond the molecular model in its current formulation, as only the interactions of the bound valence electrons are considered in the model. An *ab initio* study[49] has yielded $f_{\text{core}}\approx-1.7$ MHz, but no *ab initio* calculation of the vibrationally corrected f_{vib} has been conducted to date. Although f_{vib} is likely to be much smaller than f_{core}, the calculation of f_{vib} will provide a more complete *ab initio* model of the magnetic hyperfine parameters. Likewise, an extension of the molecular model to describe f_{core} will also provide further insight into the interactions between the nucleus and the core electrons.

The electronic component of the electric hyperfine interaction $\hat{V}_{ehf}$ can be written as a sum of products of orbital electronic and nuclear tensor operators. Analogous to the interaction of the ground-state spin with electric and strain fields, at zero order in the spin coupling coefficients, only the terms of $\hat{V}_{ehf}$ that contain A_1 orbital electronic tensor operators will have nonzero matrix elements, and these matrix elements will be diagonal and identical for each spin state. The symmetry of the lattice ensures that only similar terms from the lattice electron and internuclear contribution are also nonzero. Consequently, the electric hyperfine interaction within the ground-state spin reduces to

$$\hat{V}_{ehf}=\frac{q_z}{4Z_N}\sum_\alpha3u_{\alpha,z}^2-|\vec{u}_\alpha|^2,\tag{28}$$

where $q_z=2\langle e||\partial^2\hat{V}_e/\partial R_{N,z}^2|_{\vec{R}_0}||e\rangle+2\langle a_1||\partial^2\hat{V}_e/\partial R_{N,z}^2|_{\vec{R}_0}||a_1\rangle+\partial^2V_l/\partial R_{N,z}^2|_{\vec{R}_0}$ is proportional to the axial gradient of the net axial electric field at the ^{14}N nucleus generated by all of the electrons and other nuclei.

As per standard practice, the nuclear quadrupole operator $\sum_\alpha3u_{\alpha,z}-|\vec{u}_\alpha|^2$ can be replaced by a nuclear spin operator $Q_zI_z^2/\hbar^2$ of the same symmetry through the definition of the proportionality constant $Q_z=\langle1,1|\sum_\alpha3u_{\alpha,z}-|\vec{u}_\alpha|^2|1,1\rangle$ using the I_z eigenstate $|I=1,m_I=1\rangle$.[65] Q_z therefore quantifies the difference in the axial anisotropy of the nuclear quadrupole moment between the $m_I=\pm1$ and 0 states. The final form of the effective electric hyperfine interaction is then $\hat{V}_{ehf}=PI_z^2/\hbar^2$, where $P=q_zQ_z/4Z_N$ is the nuclear quadrupole parameter contained in Table III.

The zero-field spin Hamiltonian of the ground-state spin, including the expressions obtained for the magnetic and electric hyperfine interactions, is

$$\hat{H}_{hf}=\frac{1}{\hbar^2}\left[D_{gs}S_z^2+A_\parallel S_zI_z+A_\perp(S_xI_x+S_yI_y)+PI_z^2\right].\tag{29}$$

The approximate solutions of $\hat{H}_{hf}$ can be obtained by constructing the hyperfine states of the ground triplet in a similar manner to the earlier construction of the electronic spin-orbit states by defining linear combinations of products of electronic spin orbit and nuclear spin states that have definite C_{3v} symmetry. Given that the symmetrized nuclear

spin states of the ^{14}N nucleus in terms of the I_z eigenstates $\{|I,m_I\rangle\}$ are $I_{A_2} = |1,0\rangle$, $I_{E,x} = \frac{-i}{\sqrt{2}}(|1,1\rangle + |1,-1\rangle)$, and $I_{E,y} = \frac{-1}{\sqrt{2}}(|1,1\rangle - |1,-1\rangle)$, the symmetrized hyperfine states $\Psi_{n,j,k}$ are

$$\Psi_{1,E,x} = \Phi^{so}_{1,A_1} I_{E,x},\ \Psi_{1,E,y} = \Phi^{so}_{1,A_1} I_{E,y}, \quad \Psi_{2,A_2} = \Phi^{so}_{2,A_1} I_{A_2},$$
$$\Psi_{3,E,x} = \frac{1}{\sqrt{2}}\left(\Phi^{so}_{2,E,x} I_{E,x} - \Phi^{so}_{2,E,y} I_{E,y}\right),$$
$$\Psi_{3,E,y} = \frac{-1}{\sqrt{2}}\left(\Phi^{so}_{2,E,x} I_{E,y} + \Phi^{so}_{2,E,y} I_{E,x}\right),$$
$$\Psi_{4,A_1} = \frac{1}{\sqrt{2}}\left(\Phi^{so}_{2,E,x} I_{E,x} + \Phi^{so}_{2,E,y} I_{E,y}\right),$$
$$\Psi_{5,A_2} = \frac{1}{\sqrt{2}}\left(\Phi^{so}_{2,E,x} I_{E,y} - \Phi^{so}_{2,E,y} I_{E,x}\right),$$
$$\Psi_{6,E,x} = -\Phi^{so}_{2,E,y} I_{A_2},\ \Psi_{6,E,y} = \Phi^{so}_{2,E,x} I_{A_2}. \tag{30}$$

The matrix representation of the zero-field Hamiltonian in the basis of hyperfine states $\{\Psi_{2,A_2}, \Psi_{6,E,x}, \Psi_{6,E,y}, \Psi_{1,E,x}, \Psi_{1,E,y}, \Psi_{3,E,x}, \Psi_{3,E,y}, \Psi_{4,A_1}, \Psi_{5,A_2}\}$ is

$$H_{hf} = \begin{pmatrix} 0 & 0 & 0 & 0 & 0 & 0 & 0 & 0 & \sqrt{2}A_\perp \\ 0 & D_{gs} & 0 & -A_\perp & 0 & 0 & 0 & 0 & 0 \\ 0 & 0 & D_{gs} & 0 & -A_\perp & 0 & 0 & 0 & 0 \\ 0 & -A_\perp & 0 & P & 0 & 0 & 0 & 0 & 0 \\ 0 & 0 & -A_\perp & 0 & P & 0 & 0 & 0 & 0 \\ 0 & 0 & 0 & 0 & 0 & D_{gs}+h_+ & 0 & 0 & 0 \\ 0 & 0 & 0 & 0 & 0 & 0 & D_{gs}+h_+ & 0 & 0 \\ 0 & 0 & 0 & 0 & 0 & 0 & 0 & D_{gs}+h_- & 0 \\ \sqrt{2}A_\perp & 0 & 0 & 0 & 0 & 0 & 0 & 0 & D_{gs}+h_- \end{pmatrix}, \tag{31}$$

where $h_\pm = P \pm A_\parallel$. Note that the above basis of hyperfine states has been grouped into states of the same nuclear spin projection. The energies E^{hf}_n correct to first order in nuclear hyperfine interactions can be easily inferred: $E^{hf}_1 = P$, $E^{hf}_2 = 0$, $E^{hf}_3 = D_{gs} + P + A_\parallel$, $E^{hf}_4 = E^{hf}_5 = D_{gs} + P - A_\parallel$, $E^{hf}_6 = D_{gs}$; and the corresponding hyperfine structure is depicted in Fig. 3. Since $A_\perp$ is observed to satisfy $A_\perp \ll D_{gs}$,[40,51] the nonaxial magnetic hyperfine parameter that couples hyperfine states of different nuclear spin projection will have a negligible effect on the zero-field hyperfine structure and state couplings.

The matrix representation of the electronic interaction with electric, magnetic, and strain fields in the hyperfine basis is

$$V_{\rm mag} + V_{\rm el} + V_{\rm str} = \begin{pmatrix} 0 & i\mathcal{B}_x & i\mathcal{B}_y & 0 & 0 & 0 & 0 & 0 & 0 \\ -i\mathcal{B}_x & d_\parallel \Pi_z - \mathcal{E}_x & \mathcal{E}_y - i\mathcal{B}_z & 0 & 0 & 0 & 0 & 0 & 0 \\ -i\mathcal{B}_y & i\mathcal{B}_z + \mathcal{E}_y & d_\parallel \Pi_z + \mathcal{E}_x & 0 & 0 & 0 & 0 & 0 & 0 \\ 0 & 0 & 0 & 0 & 0 & \frac{i\mathcal{B}_y}{\sqrt{2}} & \frac{i\mathcal{B}_x}{\sqrt{2}} & \frac{i\mathcal{B}_y}{\sqrt{2}} & \frac{i\mathcal{B}_x}{\sqrt{2}} \\ 0 & 0 & 0 & 0 & 0 & \frac{i\mathcal{B}_x}{\sqrt{2}} & -\frac{i\mathcal{B}_y}{\sqrt{2}} & -\frac{i\mathcal{B}_x}{\sqrt{2}} & \frac{i\mathcal{B}_y}{\sqrt{2}} \\ 0 & 0 & 0 & -\frac{i\mathcal{B}_y}{\sqrt{2}} & -\frac{i\mathcal{B}_x}{\sqrt{2}} & d_\parallel \Pi_z & i\mathcal{B}_z & \mathcal{E}_x & \mathcal{E}_y \\ 0 & 0 & 0 & -\frac{i\mathcal{B}_x}{\sqrt{2}} & \frac{i\mathcal{B}_y}{\sqrt{2}} & -i\mathcal{B}_z & d_\parallel \Pi_z & \mathcal{E}_y & -\mathcal{E}_x \\ 0 & 0 & 0 & -\frac{i\mathcal{B}_y}{\sqrt{2}} & \frac{i\mathcal{B}_x}{\sqrt{2}} & \mathcal{E}_x & \mathcal{E}_y & d_\parallel \Pi_z & i\mathcal{B}_z \\ 0 & 0 & 0 & -\frac{i\mathcal{B}_x}{\sqrt{2}} & -\frac{i\mathcal{B}_y}{\sqrt{2}} & \mathcal{E}_y & -\mathcal{E}_x & -i\mathcal{B}_z & d_\parallel \Pi_z \end{pmatrix}. \tag{32}$$

For magnetic fields where the ^{14}N nuclear Zeeman interaction is much smaller than the NV$^-$ hyperfine interactions ($\mu_N g_N B \ll P, h_\pm$), the nuclear Zeeman interaction may be ignored. For such magnetic fields, the above matrix representation demonstrates that the fields do not couple states of different nuclear spin projection. Furthermore, by comparing the above matrix representation with that of $\hat{H}_{gs}$, the representation also demonstrates that the hyperfine states of nuclear spin projection $m_I = 0$ (upper 3×3 diagonal block) interact with the fields in a manner similar to the electronic spin-orbit states discussed in the previous section, whereas the $m_I = \pm 1$ hyperfine states (lower 6×6 diagonal block) interact differently in the weak-field limit, where the fields induce shifts comparable to the hyperfine splittings. For example, as depicted in Fig. 3, the ($m_s = \pm 1$, $m_I = 0$) states split linearly in the presence of a nonaxial electric-strain field, whereas the nondegenerate ($m_s = \pm 1$, $m_I = \pm 1$) states repel quadratically in the presence of nonaxial electric-strain fields that satisfy $\mathcal{E}_\perp < 2A_\parallel$. Note that in the large field limit, where the fields induce shifts much larger than the hyperfine

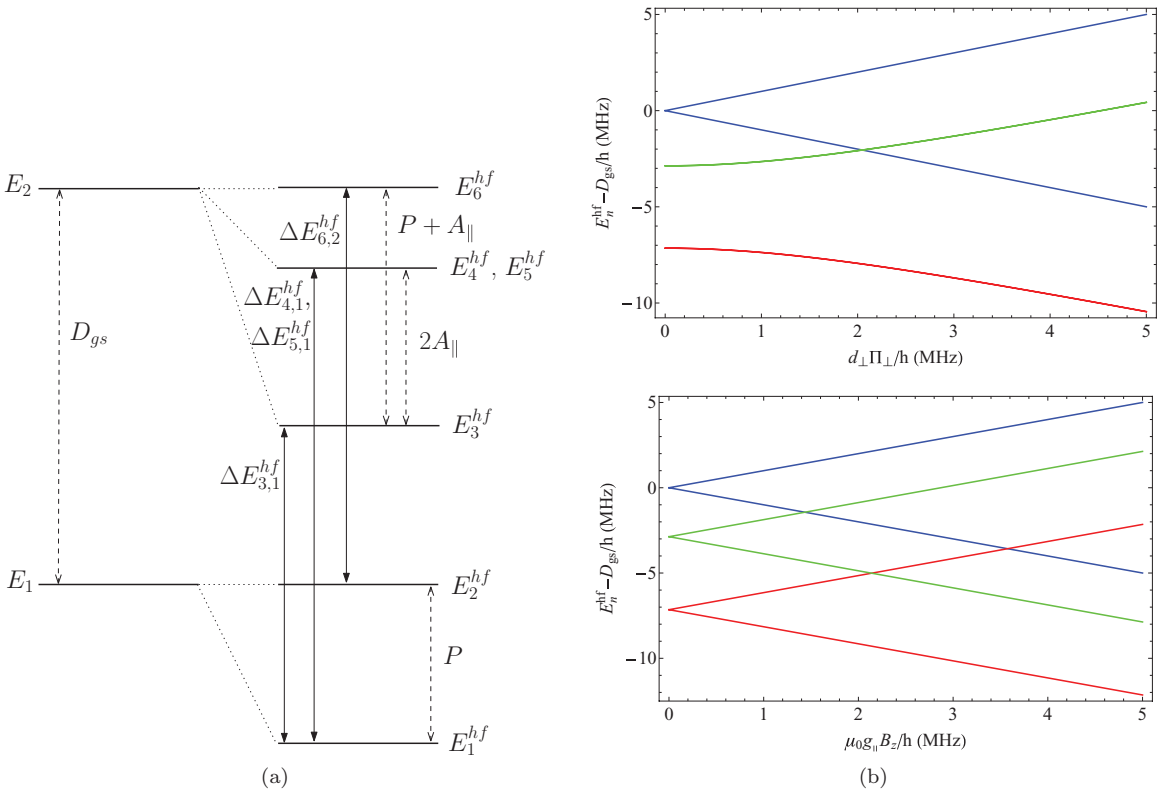

FIG. 3. (Color online) (a) The hyperfine structure of the ground triplet. The level splittings are indicated by dashed arrows and the observed values for the hyperfine parameters $A_\parallel$ and P are contained in Table III. The ordering of the hyperfine levels is based upon the parameters measured in Ref. 51. The allowed magnetic transitions between levels of the same nuclear spin projection are indicated by solid arrows and labeled by their transition energy $\Delta E_{n,m}^{hf}$. (b) The splittings of the $m_s = \pm 1$ hyperfine levels in the presence of nonaxial electric-strain fields of magnitude $\Pi_\perp$ (upper) and axial magnetic fields B_z (lower). $m_I = 0$ hyperfine levels are colored blue and $m_I = \pm 1$ hyperfine levels are colored red and green. The hyperfine parameters of Ref. 51 have been used to calculate the splittings.

splittings, both sets of hyperfine states behave approximately analogous to the spin-orbit states.

The allowed magnetic transitions are depicted in Fig. 3 and indicate that in the absence of static fields, there will exist three lines in the hyperfine spectra with energies $\Delta E_{3,1}^{hf} = D_{gs} + A_\parallel$, $\Delta E_{4,1}^{hf} = \Delta E_{5,1}^{hf} = D_{gs} - A_\parallel$, and $\Delta E_{6,2}^{hf} = D_{gs}$ in agreement with observation.[50] The central hyperfine line therefore corresponds to transitions between $m_I = 0$ states and the lower and higher energy lines correspond to transitions between $m_I = \pm 1$ states. Consequently, due to the different interactions of the $m_I = 0$ and ± 1 states in the weak static field limit, the central hyperfine line will depend differently on the static fields compared to the lower and higher energy lines. These differences in the dependence of the hyperfine lines in the weak field limit were used in the recent electric field sensing demonstration,[12] where the magnetic field was precisely aligned in the nonaxial direction ($B_z = 0$) in the presence of a nonaxial electric-strain field by observing the splitting of the $m_I = \pm 1$ hyperfine lines, while the measurement of the electric field was conducted by observing the linear splitting of the central $m_I = 0$ hyperfine line. Hence, it is clear that the hyperfine structure of the ground-state spin and its more complicated interactions with electric, magnetic, and strain fields is an important consideration for applications of the spin that operate in the weak field limit.

IV. SOLUTIONS OF THE GROUND-STATE SPIN

In this section, approximate solutions of the derived ground-state spin Hamiltonian $\hat{H}_{gs}$ will be obtained for a general electric-magnetic-strain field configuration. In later sections, these solutions will be applied to model the time evolution of the spin in a simple FID ODMR experiment and to investigate the combined effects of the fields on the spin's relaxation and inhomogeneous dephasing. As discussed in the last section, the solutions of $\hat{H}_{gs}$ describe both the interactions of the electronic spin-orbit states in the high field limit, where the field-induced shifts are much larger than the spin's hyperfine structure, and also the interactions of the $m_I = 0$ subset of hyperfine states in the weak field limit, where the field-induced shifts are comparable to the spin's hyperfine structure.

It is convenient to define the field spin states $\{|0\rangle, |-\rangle, |+\rangle\}$ in terms of the S_z eigenstates $\{|S, m_s\rangle\}$ as

$$\begin{aligned} |0\rangle &= |1,0\rangle, \\ |-\rangle &= e^{i\frac{\phi_\mathcal{E}}{2}} \sin\frac{\theta}{2}|1,1\rangle + e^{-i\frac{\phi_\mathcal{E}}{2}} \cos\frac{\theta}{2}|1,-1\rangle, \\ |+\rangle &= e^{i\frac{\phi_\mathcal{E}}{2}} \cos\frac{\theta}{2}|1,1\rangle - e^{-i\frac{\phi_\mathcal{E}}{2}} \sin\frac{\theta}{2}|1,-1\rangle, \end{aligned} \tag{33}$$

where $\tan\phi_\mathcal{E} = \mathcal{E}_y/\mathcal{E}_x$, $\tan\theta = \mathcal{E}_\perp/\mathcal{B}_z$, and $\mathcal{E}_\perp = \sqrt{\mathcal{E}_x^2 + \mathcal{E}_y^2}$. The matrix representation of $\hat{H}_{gs}$ in the basis $\{|0\rangle, |-\rangle, |+\rangle\}$ is

$$H_{gs} = \begin{pmatrix} 0 & \frac{\mathcal{B}_\perp}{\sqrt{2}}\left(e^{i\frac{\phi}{2}}s_{\frac{\theta}{2}} + e^{-i\frac{\phi}{2}}c_{\frac{\theta}{2}}\right) & \frac{\mathcal{B}_\perp}{\sqrt{2}}\left(e^{i\frac{\phi}{2}}c_{\frac{\theta}{2}} - e^{-i\frac{\phi}{2}}s_{\frac{\theta}{2}}\right) \\ \frac{\mathcal{B}_\perp}{\sqrt{2}}\left(e^{-i\frac{\phi}{2}}s_{\frac{\theta}{2}} + e^{i\frac{\phi}{2}}c_{\frac{\theta}{2}}\right) & \mathcal{D}-\mathcal{R} & 0 \\ \frac{\mathcal{B}_\perp}{\sqrt{2}}\left(e^{-i\frac{\phi}{2}}c_{\frac{\theta}{2}} - e^{i\frac{\phi}{2}}s_{\frac{\theta}{2}}\right) & 0 & \mathcal{D}+\mathcal{R} \end{pmatrix}, \tag{34}$$

where $\phi = 2\phi_{\mathcal{B}} + \phi_{\mathcal{E}}$, $\tan\phi_{\mathcal{B}} = \mathcal{B}_y/\mathcal{B}_x$, $\mathcal{R} = \sqrt{\mathcal{B}_z^2 + \mathcal{E}_\perp^2}$, $c_{\frac{\theta}{2}} = \cos\frac{\theta}{2}$, and $s_{\frac{\theta}{2}} = \sin\frac{\theta}{2}$. Therefore, if $\mathcal{B}_\perp = \sqrt{\mathcal{B}_x^2 + \mathcal{B}_y^2} \ll \mathcal{D}$ and $\mathcal{B}_\perp^2/\mathcal{D} \ll \mathcal{R}$, the field spin states are approximate eigenstates of $\hat{H}_{gs}$ with energies $E_0 = 0$ and $E_\pm = \mathcal{D} \pm \mathcal{R}$. In this weak nonaxial magnetic field limit, the spin eigenstates are completely characterized by the field angles $\phi_{\mathcal{E}}$ and θ derived from the axial magnetic and nonaxial electric-strain field components, and the energy splitting of the $|\pm\rangle$ states is governed by the magnitudes of the same field components.

When $\mathcal{B}_\perp^2/\mathcal{D} \sim \mathcal{R}$, first-order corrections to the field spin states become important, such that

$$\begin{aligned} |0\rangle^{(1)} &= |0\rangle - \sqrt{\frac{\Delta\mathcal{R}}{\mathcal{D}}}\left(e^{-i\frac{\phi}{2}}s_{\frac{\theta}{2}} + e^{i\frac{\phi}{2}}c_{\frac{\theta}{2}}\right)|-\rangle - \sqrt{\frac{\Delta\mathcal{R}}{\mathcal{D}}}\left(e^{-i\frac{\phi}{2}}c_{\frac{\theta}{2}} - e^{i\frac{\phi}{2}}s_{\frac{\theta}{2}}\right)|+\rangle, \\ |-\rangle^{(1)} &= |-\rangle + \sqrt{\frac{\Delta\mathcal{R}}{\mathcal{D}}}\left(e^{i\frac{\phi}{2}}s_{\frac{\theta}{2}} + e^{-i\frac{\phi}{2}}c_{\frac{\theta}{2}}\right)|0\rangle, \quad |+\rangle^{(1)} = |+\rangle + \sqrt{\frac{\Delta\mathcal{R}}{\mathcal{D}}}\left(e^{i\frac{\phi}{2}}c_{\frac{\theta}{2}} - e^{-i\frac{\phi}{2}}s_{\frac{\theta}{2}}\right)|0\rangle, \end{aligned} \tag{35}$$

where $\Delta = \mathcal{B}_\perp^2/2\mathcal{R}\mathcal{D}$, and second-order perturbation corrections to the energies also become important, such that $E_0^{(2)} = -\Delta\mathcal{R}$ and

$$E_\pm^{(2)} = \mathcal{D} + \Delta\mathcal{R} \pm \mathcal{R}(1 - 2\Delta\sin\theta\cos\phi + \Delta^2)^{\frac{1}{2}}. \tag{36}$$

Consequently, in the strong nonaxial magnetic field limit, the spin eigenstates and energies become dependent on the nonaxial magnetic field direction $\phi_{\mathcal{B}}$ and the dimensionless ratio of the field magnitudes Δ.

Figure 4 contains polar plots of the dimensionless splitting parameter $(1 - 2\Delta\sin\theta\cos\phi + \Delta^2)^{\frac{1}{2}}$ of the $|\pm\rangle$ spin states as a function of the azimuthal ϕ and polar θ field angles. Clearly, the most interesting field configurations have the parameters $\Delta \sim 1$ and $\theta \sim \frac{\pi}{2}$ since for these parameters the energies depend sensitively on the field angles. Such a field configuration was used in the recent electric field sensing demonstration[12] to sensitively detect both the magnitude and orientation of an applied electric field. Future implementations of the ground-state spin as a field sensor should seek to exploit these high-sensitivity field configurations.

The matrix representation of the interaction of the ground-state spin with an oscillating microwave magnetic field $\vec{M}$ in the basis $\{|0\rangle,|-\rangle,|+\rangle\}$ is

$$\frac{1}{\hbar}\vec{S}\cdot\vec{\mathcal{M}} = \begin{pmatrix} 0 & \frac{\mathcal{M}_\perp}{\sqrt{2}}\left(e^{i\frac{\phi_m}{2}}s_{\frac{\theta}{2}} + e^{-i\frac{\phi_m}{2}}c_{\frac{\theta}{2}}\right) & \frac{\mathcal{M}_\perp}{\sqrt{2}}\left(e^{i\frac{\phi_m}{2}}c_{\frac{\theta}{2}} - e^{-i\frac{\phi_m}{2}}s_{\frac{\theta}{2}}\right) \\ \frac{\mathcal{M}_\perp}{\sqrt{2}}\left(e^{-i\frac{\phi_m}{2}}s_{\frac{\theta}{2}} + e^{i\frac{\phi_m}{2}}c_{\frac{\theta}{2}}\right) & -\mathcal{M}_z\cos\theta & \mathcal{M}_z\sin\theta \\ \frac{\mathcal{M}_\perp}{\sqrt{2}}\left(e^{-i\frac{\phi_m}{2}}c_{\frac{\theta}{2}} - e^{i\frac{\phi_m}{2}}s_{\frac{\theta}{2}}\right) & \mathcal{M}_z\sin\theta & \mathcal{M}_z\cos\theta \end{pmatrix},$$

where $\mathcal{M}_z = \mu_B g_\parallel M_z$, $\mathcal{M}_x = \mu_B g_\perp M_x$, $\mathcal{M}_y = \mu_B g_\perp M_y$, $\mathcal{M}_\perp = \sqrt{\mathcal{M}_x^2 + \mathcal{M}_y^2}$, $\phi_m = 2\phi_{\mathcal{M}} + \phi_{\mathcal{E}}$, and $\tan\phi_{\mathcal{M}} = \mathcal{M}_y/\mathcal{M}_x$. The off diagonals of the above matrix representation indicate that the transitions between the field spin states induced by the oscillating microwave field are also dependent on the static field angles.

Using Fermi's golden rule,[59] the transition rates $W_{0\to\pm}$ between the $|0\rangle$ and $|\pm\rangle$ spin states correct to zero order in the static nonaxial magnetic field $\mathcal{B}_\perp$ are proportional to the absolute square of the off-diagonal elements, such that

$$W_{0\to\pm} \propto \tfrac{1}{2}\mathcal{M}_\perp^2(1 \mp \sin\theta\cos\phi_m). \tag{37}$$

As the transition rates to the $|\pm\rangle$ spin states depend differently on the static fields for a given microwave polarization, the transitions to the $|\pm\rangle$ spin states can be controlled via the static fields, or conversely for a given static field configuration, the transitions can be controlled via the microwave polarization. Figure 5 depicts the dependence of the transition rates on the microwave polarization and static field configuration. As can be seen, the individual transitions can be selectively excited using orthogonal nonaxial microwave polarizations $\phi_{\mathcal{M}} = \frac{\phi_{\mathcal{E}}}{2}, \frac{\phi_{\mathcal{E}}}{2} + \frac{\pi}{2}$ when $\theta \sim \frac{\pi}{2}$. Hence, linearly polarized microwaves in conjunction with static field control or (as has been previously demonstrated)[66] circularly polarized microwaves can be used to selectively excite individual spin transition in situations where the splitting of the $|\pm\rangle$ spin states ($= 2\mathcal{R}$) is too small to selectively excite the individual transitions using microwave frequency selection alone.

V. TIME EVOLUTION OF THE SPIN: FID SIMULATION

Assuming the weak static nonaxial magnetic field limit ($\mathcal{B}_\perp \ll \mathcal{D}$ and $\mathcal{B}_\perp^2/\mathcal{D} \ll \mathcal{R}$), which typically occurs in most of the current applications of the ground-state spin, the spin solutions can be used to accurately model the time evolution of the spin in a simple FID ODMR experiment. As depicted

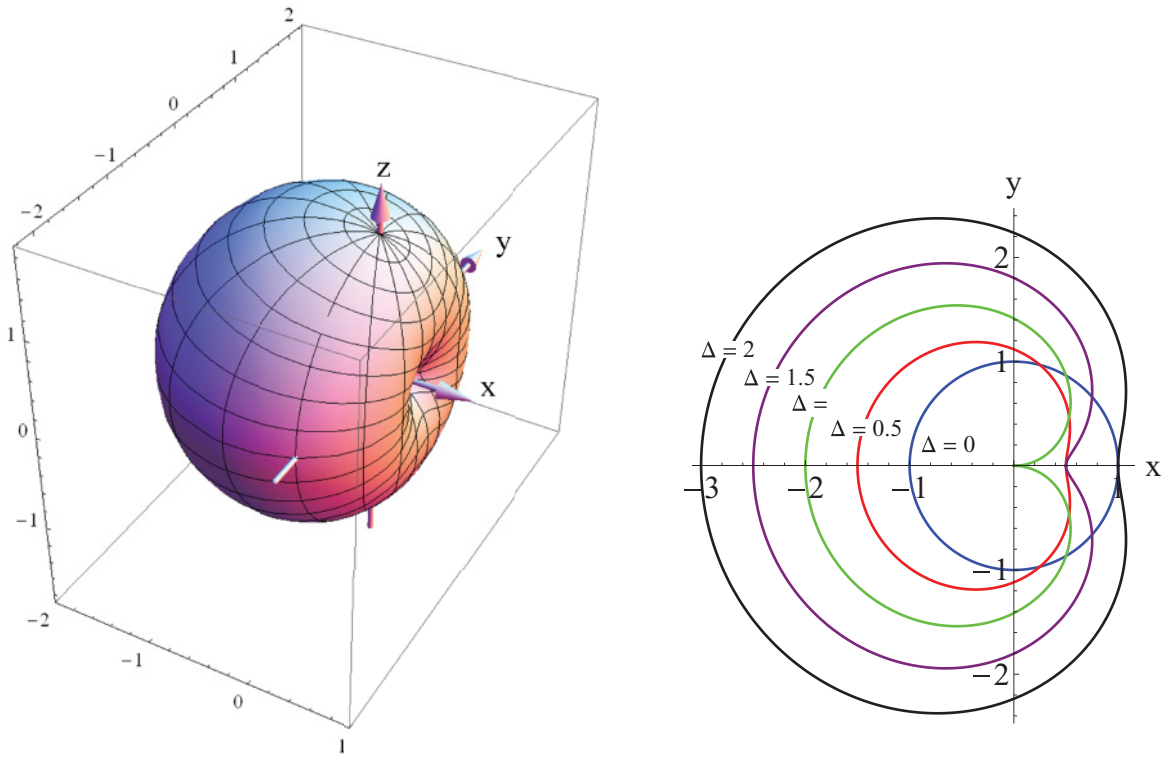

FIG. 4. (Color online) Plots of the dimensionless energy splitting parameter $(1 - 2\Delta \sin\theta \cos\phi + \Delta^2)^{\frac{1}{2}}$ of the $|\pm\rangle$ spin states as (a) a function of the azimuthal $0 \leqslant \phi \leqslant 2\pi$ and polar $0 \leqslant \theta \leqslant \pi$ field angles for $\Delta = 1$; and (b) as a function of ϕ for $\theta = \frac{\pi}{2}$ and different values of Δ as indicated. Coordinate axes are provided for reference to Fig. 1 where the field angles $\phi = 2\phi_{\mathcal{B}} + \phi_{\mathcal{E}}$, $\phi_{\mathcal{E}}$, $\phi_{\mathcal{B}}$, and θ are defined.

in Fig. 6, the FID sequence is comprised of optical pulses that polarize the spin at $t = -t_r$ and read out the spin at $t = t_r$, as well as microwave $\pi/2$ pulses that coherently manipulate the spin before and after the period of free evolution τ. Note that the MW pulse sequence depicted in Fig. 6 differs from the conventional ESR sequence by the final $\pi/2$ pulse, which projects the accumulated phase into a population difference between the $m_s = 0$ and ± 1 spin sublevels.

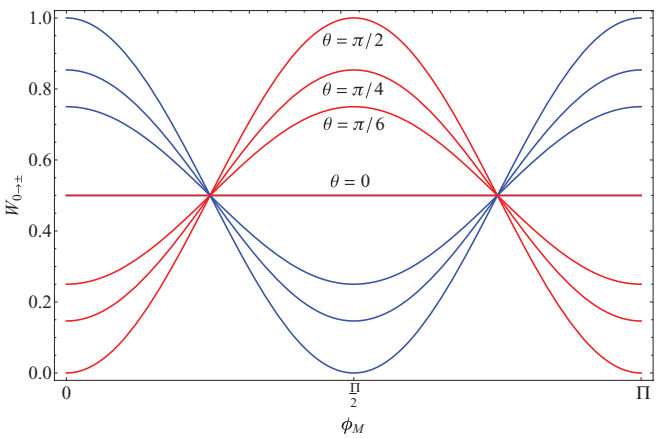

FIG. 5. (Color online) Plots of the normalized transition rates $W_{0\to-} \propto \frac{1}{2}(1 + \sin\theta \cos\phi_m)$ (blue) and $W_{0\to+} \propto \frac{1}{2}(1 - \sin\theta \cos\phi_m)$ (red) between the $|0\rangle$ and $|-\rangle$ and the $|0\rangle$ and $|+\rangle$ spin states, respectively, as functions of the nonaxial microwave polarization $\phi_{\mathcal{M}}$, given $\phi_{\mathcal{E}} = 0$ and different values of the static field angle θ. Note that the transition rates are equal for all values of $\phi_{\mathcal{M}}$ when $\theta = 0$.

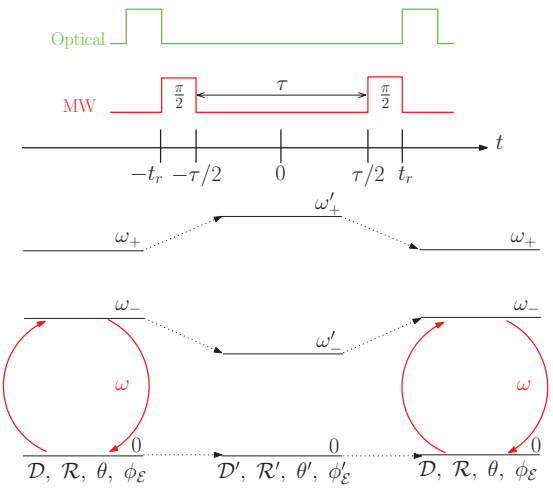

FIG. 6. (Color online) The free induction decay (FID) sequence of optical pulses that polarize the spin at $t = -t_r$ and read out the spin at $t = t_r$, as well as microwave $\pi/2$ pulses that coherently manipulate the spin before and after the period of free evolution τ. The static fields and spin state energies differ during the period of free evolution $(\mathcal{D}', \mathcal{R}', \theta', \phi'_{\mathcal{E}}, \hbar\omega'_{\pm})$ compared to before and after the period of free evolution $(\mathcal{D}, \mathcal{R}, \theta, \phi_{\mathcal{E}}, \hbar\omega_{\pm})$. The microwave field is assumed to selectively excite the transitions between the $|0\rangle$ and $|-\rangle$ spin states with frequency ω.

In the model of the FID experiment, the static fields will be considered to differ during the period of free evolution, such that before and after the period of free evolution the static fields are described by the parameters ($\mathcal{D}$, $\mathcal{R}$, θ, $\phi_{\mathcal{E}}$) and the $|\pm\rangle$ spin states have energies $\hbar\omega_{\pm}$, while during the period of free evolution the static fields are described by the parameters ($\mathcal{D}'$, $\mathcal{R}'$, θ', $\phi'_{\mathcal{E}}$) and the $|\pm\rangle$ spin states have energies $\hbar\omega'_{\pm}$. For simplicity, the changes in the static field configurations are assumed to be adiabatic and infinitely sharp at $t = \pm\tau/2$, and the microwave field is assumed to selectively excite the transitions between the $|0\rangle$ and $|-\rangle$ spin states with a tuned microwave frequency $\omega \approx \omega_-$.

This model FID experiment is a generalization of the FID experiments that were conducted in the spin's recent electric field sensing demonstration[12] and one of the spin's magnetic field sensing demonstrations[5] and will consequently describe how the combined effects of electric, magnetic, and strain fields will influence such sensing demonstrations. However, note that the objective of presenting this model FID experiment in this work is not to discuss sensing techniques, but to provide the necessary theoretical details to discuss the effects of inhomogeneous fields and lattice interactions on the relaxation and dephasing of the spin in the following sections.

The state of the spin at a given time during the FID sequence $|t\rangle$ can be written in terms of the spin eigenstates of the static fields at that time:

$$|t\rangle = \begin{cases} c_0(t)|0\rangle + c_-(t)|-\rangle + c_+(t)|+\rangle, & -t_r \leqslant t \leqslant -\frac{\tau}{2}, \\ & \frac{\tau}{2} \leqslant t \leqslant t_r \\ c'_0(t)|0\rangle' + c'_-(t)|-\rangle' + c'_+(t)|+\rangle', & -\frac{\tau}{2} < t < \frac{\tau}{2} \end{cases} \tag{38}$$

where the coefficients $c_i(t)$ and $c'_i(t)$ ($i = 0, -, +$) are related at $t = \pm\tau/2$ by the basis transformation $\mathcal{T} : \{|0\rangle, |-\rangle, |+\rangle\} \rightarrow \{|0\rangle', |-\rangle', |+\rangle'\}$ given by the matrix

$$\mathcal{T} = \begin{pmatrix} 1 & 0 & 0 \\ 0 & c_{\delta\phi_{\mathcal{E}}} c_{\delta\theta_-} - i s_{\delta\phi_{\mathcal{E}}} c_{\delta\theta_+} & -c_{\delta\phi_{\mathcal{E}}} s_{\delta\theta_-} + i s_{\delta\phi_{\mathcal{E}}} s_{\delta\theta_+} \\ 0 & c_{\delta\phi_{\mathcal{E}}} s_{\delta\theta_-} + i s_{\delta\phi_{\mathcal{E}}} s_{\delta\theta_+} & c_{\delta\phi_{\mathcal{E}}} c_{\delta\theta_-} + i s_{\delta\phi_{\mathcal{E}}} c_{\delta\theta_+} \end{pmatrix}, \tag{39}$$

where $\delta\phi_{\mathcal{E}} = \frac{1}{2}(\phi'_{\mathcal{E}} - \phi_{\mathcal{E}})$ and $\delta\theta_{\pm} = \frac{1}{2}(\theta' \pm \theta)$.

Introducing the density operator $\hat{\rho}(t) = |t\rangle\langle t|$, the matrix representation of $\hat{\rho}(t)$ in the spin eigenstate basis of the fields at t ($\{|0\rangle, |-\rangle, |+\rangle\}$ or $\{|0\rangle', |-\rangle', |+\rangle'\}$) is

$$\hat{\rho}(t) = \begin{cases} \rho(t), & -t_r \leqslant t \leqslant -\frac{\tau}{2}, \frac{\tau}{2} \leqslant t \leqslant t_r \\ \rho'(t), & -\frac{\tau}{2} < t < \frac{\tau}{2} \end{cases} \tag{40}$$

where the elements of the matrices $\rho(t)$ and $\rho'(t)$ are $\rho_{ij}(t) = c_i(t)c_j^*(t)$ and $\rho'_{ij}(t) = c'_i(t)c'^*_j(t)$, respectively, and at $t = \pm\frac{\tau}{2}$ the matrices are related by the transformations $\rho'(-\frac{\tau}{2}) = \mathcal{T}^{-1}\rho(-\frac{\tau}{2})\mathcal{T}$ and $\rho(\frac{\tau}{2}) = \mathcal{T}\rho'(\frac{\tau}{2})\mathcal{T}^{-1}$.

In order to simplify the treatment of the interaction of the spin with the microwave pulses, the rotating wave approximation can be adopted and the density operator transformed into the rotating reference frame, such that $\rho(t) \rightarrow \tilde{\rho}(t)$ and $\rho'(t) \rightarrow \tilde{\rho}'(t)$, where $\tilde{\rho}^*_{\pm 0}(t) = \tilde{\rho}_{0\pm}(t) = \rho_{0\pm}(t)e^{-i\omega t}$, $\tilde{\rho}'^*_{\pm 0}(t) = \tilde{\rho}'_{0\pm}(t) = \rho'_{0\pm}(t)e^{-i\omega t}$, and $\tilde{\rho}_{ij}(t) = \rho_{ij}(t)$ and $\tilde{\rho}'_{ij}(t) = \rho'_{ij}(t)$ for the other density matrix elements.[67] The effect of the $\pi/2$ microwave pulses can therefore be described by $\tilde{\rho}(-\frac{\tau}{2}) = e^{-iJ\frac{\pi}{2}}\tilde{\rho}(-t_r)e^{iJ\frac{\pi}{2}}$ and $\tilde{\rho}(t_r) = e^{-iJ\frac{\pi}{2}}\tilde{\rho}(\frac{\tau}{2})e^{iJ\frac{\pi}{2}}$, where using the microwave matrix representation (37),

$$J = \frac{1}{2}\begin{pmatrix} 0 & e^{i\Omega} & 0 \\ e^{-i\Omega} & 0 & 0 \\ 0 & 0 & \frac{4}{\pi}\delta\omega_{+-}\delta t_{\frac{\pi}{2}} \end{pmatrix}, \tag{41}$$

$\tan\Omega = \frac{\sin(\frac{\theta}{2} - \frac{\pi}{4})}{\sin(\frac{\theta}{2} + \frac{\pi}{4})} \tan\frac{\phi_m}{2}$, $\delta\omega_{+-} = \omega_+ - \omega_-$, and $\delta t_{\frac{\pi}{2}}$ is the duration of the $\pi/2$ pulse.

Due to the process of optical spin polarization, the first optical pulse of the FID sequence will incoherently polarize the ground-state spin such that, at $t = -t_r$,

$$\tilde{\rho}(-t_r) = \begin{pmatrix} p_0 & 0 & 0 \\ 0 & p_- & 0 \\ 0 & 0 & p_+ \end{pmatrix}, \tag{42}$$

where p_i are the populations of the spin sublevels and $p_0 + p_- + p_+ = 1$. Note that since it is believed that the spin-polarization process does not discriminate between the population of the $m_s = \pm 1$ sublevels, it is expected that $p_+ \approx p_-$. The effect of the first $\pi/2$ microwave pulse is

$$\begin{aligned} \tilde{\rho}\left(-\frac{\tau}{2}\right) &= e^{-iJ\frac{\pi}{2}}\tilde{\rho}(-t_r)e^{iJ\frac{\pi}{2}} \\ &= \begin{pmatrix} p_0 - \frac{1}{2}\delta p & \frac{i}{2}e^{i\Omega}\delta p & 0 \\ \frac{-i}{2}e^{-i\Omega}\delta p & p_0 - \frac{1}{2}\delta p & 0 \\ 0 & 0 & p_- \end{pmatrix}, \end{aligned} \tag{43}$$

where $\delta p = p_0 - p_-$ and the simplifying assumption $p_+ \approx p_-$ has been made. After the sudden change in field configuration at $t = -\frac{\tau}{2}$, $\tilde{\rho}(-\frac{\tau}{2})$ is transformed into

$$\tilde{\rho}'\left(-\frac{\tau}{2}\right) = \mathcal{T}^{-1}\tilde{\rho}\left(-\frac{\tau}{2}\right)\mathcal{T} = \begin{pmatrix} p_0 - \frac{1}{2}\delta p & \frac{i}{2}e^{i\Omega}\mathcal{T}_{--}\delta p & \frac{i}{2}e^{i\Omega}\mathcal{T}_{-+}\delta p \\ \frac{-i}{2}e^{-i\Omega}\mathcal{T}^*_{--}\delta p & p_- + \frac{1}{2}|\mathcal{T}_{--}|^2\delta p & \frac{1}{2}\mathcal{T}^*_{--}\mathcal{T}_{-+}\delta p \\ \frac{-i}{2}e^{-i\Omega}\mathcal{T}^*_{-+}\delta p & \frac{1}{2}\mathcal{T}_{--}\mathcal{T}^*_{-+}\delta p & p_- + \frac{1}{2}|\mathcal{T}_{-+}|^2\delta p \end{pmatrix}, \tag{44}$$

where $\mathcal{T}_{--} = \cos\delta\phi_{\mathcal{E}}\cos\delta\theta_- - i\sin\delta\phi_{\mathcal{E}}\cos\delta\theta_+$ and $\mathcal{T}_{-+} = -\cos\delta\phi_{\mathcal{E}}\sin\delta\theta_- + i\sin\delta\phi_{\mathcal{E}}\sin\delta\theta_+$ are elements of the basis transformation matrix.

The coherent time evolution of the ground-state spin during the free evolution period is governed by the Landau–von Neumann equation $\frac{d}{dt}\hat{\rho}'(t) = \frac{i}{\hbar}[\hat{\rho}'(t), \hat{H}'_{gs}]$. However, the spin also interacts with incoherent time-dependent perturbations such as crystal

vibrations, the thermal radiation field, and fluctuating fields from local magnetic and electric impurities during the free evolution period. These incoherent perturbations induce transitions between the spin states that lead to spin relaxation γ_{ij}^{r} and dephasing rates γ_{ij}^{p}, which are characterized by the T_1 and T_2 times of the spin, respectively.[68] Accounting for both the coherent and incoherent evolution of the spin,[67] the following matrix equation is obtained:

$$\frac{d}{dt}\tilde{\rho}'(t) = \begin{pmatrix} -\left(\gamma_{0-}^{r}+\gamma_{0+}^{r}\right)\tilde{\rho}'_{00} & \left(i\delta\omega'_{-}-\gamma_{-0}^{p}\right)\tilde{\rho}'_{0-} & \left(i\delta\omega'_{+}-\gamma_{+0}^{p}\right)\tilde{\rho}'_{0+} \\ +\gamma_{-0}^{r}\tilde{\rho}'_{--}+\gamma_{+0}^{r}\tilde{\rho}'_{++} & & \\ \left(-i\delta\omega'_{-}-\gamma_{-0}^{p}\right)\tilde{\rho}'_{-0} & -\left(\gamma_{-0}^{r}+\gamma_{-+}^{r}\right)\tilde{\rho}'_{--} & (i\delta\omega'_{+-}-\gamma_{+-}^{p})\tilde{\rho}'_{-+} \\ & +\gamma_{0-}^{r}\tilde{\rho}'_{00}+\gamma_{+-}^{r}\tilde{\rho}'_{++} & \\ \left(-i\delta\omega'_{+}-\gamma_{+0}^{p}\right)\tilde{\rho}'_{+0} & (i\delta\omega'_{+-}-\gamma_{+-}^{p})\tilde{\rho}'_{+-} & -\left(\gamma_{+0}^{r}+\gamma_{+-}^{r}\right)\tilde{\rho}'_{++} \\ & & +\gamma_{0+}^{r}\tilde{\rho}'_{00}+\gamma_{-+}^{r}\tilde{\rho}'_{--} \end{pmatrix}, \tag{45}$$

where $\delta\omega'_{\pm}=\omega'_{\pm}-\omega$ and $\delta\omega'_{+-}=\omega'_{+}-\omega'_{-}$. Note that the coherent coupling between the NV^{-} spin and proximal impurity spins will not be considered in this work.

The solutions of the off-diagonal elements at $t=\frac{\tau}{2}$ are simply

$$\begin{aligned} \tilde{\rho}'^{*}_{-0}\left(\frac{\tau}{2}\right) &= \tilde{\rho}'_{0-}\left(\frac{\tau}{2}\right) = \tilde{\rho}'_{0-}\left(-\frac{\tau}{2}\right)e^{-\gamma_{-0}^{p}\tau}e^{i\delta\omega'_{-}\tau}, \\ \tilde{\rho}'^{*}_{+0}\left(\frac{\tau}{2}\right) &= \tilde{\rho}'_{0+}\left(\frac{\tau}{2}\right) = \tilde{\rho}'_{0+}\left(-\frac{\tau}{2}\right)e^{-\gamma_{+0}^{p}\tau}e^{i\delta\omega'_{+}\tau}, \\ \tilde{\rho}'^{*}_{+-}\left(\frac{\tau}{2}\right) &= \tilde{\rho}'_{-+}\left(\frac{\tau}{2}\right) = \tilde{\rho}'_{-+}\left(-\frac{\tau}{2}\right)e^{-\gamma_{+-}^{p}\tau}e^{i\delta\omega'_{+-}\tau}, \end{aligned} \tag{46}$$

while the solutions of the diagonal elements $\tilde{\rho}'_{00}(\frac{\tau}{2})$, $\tilde{\rho}'_{--}(\frac{\tau}{2})$, and $\tilde{\rho}'_{++}(\frac{\tau}{2})$ are more complicated, but can still be obtained analytically as combinations of exponential functions of the relaxation rates. It follows that after the second sudden change in the static fields at $t=\frac{\tau}{2}$, $\tilde{\rho}(\frac{\tau}{2})=\mathcal{T}\tilde{\rho}'(\frac{\tau}{2})\mathcal{T}^{-1}$, and after the second $\pi/2$ microwave pulse at $t=t_r$, $\tilde{\rho}(t_r)=e^{-iJ\frac{\pi}{2}}\tilde{\rho}(\frac{\tau}{2})e^{iJ\frac{\pi}{2}}$. The second optical pulse at $t=t_r$ reads out the proportion of the population in the $m_s=0$ sublevel, such that the optical emission intensity $I(\tau)\propto\tilde{\rho}_{00}(t_r)$, where

$$\begin{aligned} \tilde{\rho}_{00}(t_r) &= \frac{1}{2}\left[\tilde{\rho}'_{00}\left(\frac{\tau}{2}\right)+|\mathcal{T}_{--}|^2\tilde{\rho}'_{--}\left(\frac{\tau}{2}\right)+|\mathcal{T}_{-+}|^2\tilde{\rho}'_{++}\left(\frac{\tau}{2}\right)\right] \\ &\quad -\frac{\delta p}{2}[|\mathcal{T}_{--}|^2e^{-\gamma_{-0}^{p}\tau}\cos\delta\omega'_{-}\tau \\ &\quad +|\mathcal{T}_{-+}|^2e^{-\gamma_{+0}^{p}\tau}\cos\delta\omega'_{+}\tau \\ &\quad -|\mathcal{T}_{--}|^2|\mathcal{T}_{-+}|^2e^{-\gamma_{+-}^{p}\tau}\cos\delta\omega'_{+-}\tau] \\ &= \frac{1}{2}N(\tau)-\frac{\delta p}{2}O(\tau). \end{aligned} \tag{47}$$

The first term $N(\tau)$ is not oscillatory and depends only on the diagonal elements $\tilde{\rho}'_{00}(-\frac{\tau}{2})$, $\tilde{\rho}'_{--}(-\frac{\tau}{2})$, and $\tilde{\rho}'_{++}(-\frac{\tau}{2})$ and the relaxation rates γ_{ij}^{r}. The second term $O(\tau)$ has oscillatory components with frequencies corresponding to the different frequency shifts ($\delta\omega'_{\pm}$ and $\delta\omega'_{+-}$) and the contributions of each oscillatory component are dependent on the state couplings ($|\mathcal{T}_{--}|$ and $|\mathcal{T}_{-+}|$) and the dephasing rates γ_{ij}^{p}. The oscillatory term therefore offers a great deal of information about the spin eigenstates and their energies during the period of free evolution. Furthermore, since the observed T_1 and T_2 times of the ground-state spin typically differ by at least one order of magnitude,[5] the change in the nonoscillatory term over the lifetime of the oscillatory term is negligible, and thus can be effectively ignored in an observation of the oscillatory term.

The oscillatory term can be observed by conducting ODMR measurements of an ensemble of spins or conducting many ODMR measurements of a single spin. For a given measurement of an ensemble of spins, the field parameters $(\mathcal{D},\mathcal{R},\theta,\phi_{\mathcal{E}})$ and $(\mathcal{D}',\mathcal{R}',\theta',\phi'_{\mathcal{E}})$ will potentially differ for each spin within the ensemble due to inhomogeneities in the fields. Likewise, for an ensemble of measurements of a single spin, the field parameters will potentially differ between each measurement due to differences in the preparation of the spin and the fields. These ensemble inhomogeneities introduce an additional dephasing decay in the observation of the oscillatory term, and can be accounted for by introducing statistical distribution functions of the field parameters and calculating the expectation value $\langle O(\tau)\rangle$.[69]

VI. EFFECTS OF INHOMOGENEOUS FIELDS

The total dephasing rate of the spin due to interactions with incoherent time-dependent fields and inhomogeneous static fields is characterized by the T_2^* time of the spin.[68] In the recent electric field sensing demonstration,[12] it was observed that the T_2^* time of the ground-state spin was highly dependent on the field configuration, such that it obtained a maximum in the absence of an axial magnetic field and sharply decreased as the axial magnetic field was increased at a rate that was inversely related to the nonaxial electric-strain field. This observation highlighted the significant influence that the static fields have on the dephasing of the spin and the potential to control the susceptibility of the spin to different noise sources. The dephasing due to static field inhomogeneities will be discussed in this section, and the dependence of the incoherent dephasing rates γ_{ij}^{p} on the static fields will be discussed in the next section.

Since the ground-state spin interacts very weakly with axial electric-strain fields, the effect of the variation of $\mathcal{D}$ and $\mathcal{D}'$ between the measurements of a single spin will be negligible compared to the variations in the other field parameters. Note that this is not necessarily the case for an ensemble of spins because local strain fields can vary significantly between lattice sites. Nor is it necessarily the case for single spins or ensembles

of spins if temperature varies appreciably during the conduct of the measurements.[70] Nevertheless, the variations in $\mathcal{D}$ and $\mathcal{D}'$ are considered negligible in the following. It is reasonable to expect that the field parameters $\mathcal{R}$ and $\mathcal{R}'$ will have statistical distributions $f(\mathcal{R}/\hbar,\mu_{\mathcal{R}},\sigma_{\mathcal{R}})$ and $f(\mathcal{R}'/\hbar,\mu_{\mathcal{R}'},\sigma_{\mathcal{R}'})$ that have the same distribution function f, but different mean values $\mu_{\mathcal{R}}$ and $\mu_{\mathcal{R}'}$ and different variances $\sigma_{\mathcal{R}}$ and $\sigma_{\mathcal{R}'}$ in units of frequency.

The distribution functions of the frequency shifts $\delta\omega'_{\pm}$ and $\delta\omega'_{+-}$ can be constructed using the distributions of $\mathcal{R}$ and $\mathcal{R}'$ as[71]

$$\begin{aligned}
F_-(\delta\omega'_-,\mu_-,\sigma_-) &= \int_0^\infty f(\mathcal{R}/\hbar,\mu_{\mathcal{R}},\sigma_{\mathcal{R}}) \\
&\quad\times f(\delta\omega'_- + \mathcal{R}/\hbar,\mu_{\mathcal{R}'},\sigma_{\mathcal{R}'})d\mathcal{R}/\hbar, \\
F_+(\delta\omega'_+,\mu_+,\sigma_+) &= \int_0^\infty f(\mathcal{R}/\hbar,\mu_{\mathcal{R}},\sigma_{\mathcal{R}}) \\
&\quad\times f(\delta\omega'_+ - \mathcal{R}/\hbar,\mu_{\mathcal{R}'},\sigma_{\mathcal{R}'})d\mathcal{R}/\hbar, \\
F_{+-}(\delta\omega'_{+-},\mu_{+-},\sigma_{+-}) &= \frac{1}{2}f\left(\frac{1}{2}\delta\omega'_{+-},\mu_{\mathcal{R}'},\sigma_{\mathcal{R}'}\right),
\end{aligned} \tag{48}$$

where the explicit expressions for the means $\mu_{\pm}$ and μ_{+-} and the variances $\sigma_{\pm}$ and σ_{+-} in terms of $\mu_{\mathcal{R}}$, $\mu_{\mathcal{R}'}$, $\sigma_{\mathcal{R}}$, and $\sigma_{\mathcal{R}'}$ depend on the distribution f. For example, if f is the normal distribution, then the expressions are simply $\mu_{\pm} = \delta\mathcal{D}/\hbar + \mu_{\mathcal{R}} \pm \mu_{\mathcal{R}'}$, $\mu_{+-} = 2\mu_{\mathcal{R}'}$, $\sigma_{\pm} = \sigma_{\mathcal{R}} + \sigma_{\mathcal{R}'}$, and $\sigma_{+-} = 2\sigma_{\mathcal{R}'}$.[71]

Using the distributions of the frequency shifts, the expectation value of the FID oscillatory term for an ensemble of measurements of a single spin is

$$\begin{aligned}
&\langle O(\tau)\rangle \\
&= \langle|\mathcal{T}_{--}|^2\rangle e^{-\gamma^p_{-0}\tau}\int_{-\infty}^{\infty}\cos\delta\omega'_-\tau\,F_-(\delta\omega'_-,\mu_-,\sigma_-)d\delta\omega'_- \\
&\quad+\langle|\mathcal{T}_{-+}|^2\rangle e^{-\gamma^p_{+0}\tau}\int_{-\infty}^{\infty}\cos\delta\omega'_+\tau\,F_+(\delta\omega'_+,\mu_+,\sigma_+)d\delta\omega'_+ \\
&\quad-\langle|\mathcal{T}_{--}|^2|\mathcal{T}_{-+}|^2\rangle e^{-\gamma^p_{+-}\tau}\int_{-\infty}^{\infty}\frac{1}{2}\cos\delta\omega'_{+-}\tau \\
&\quad\times F_{+-}\left(\frac{1}{2}\delta\omega'_{+-},\mu_{+-},\sigma_{+-}\right)d\delta\omega'_{+-}.
\end{aligned} \tag{49}$$

Note that the expectation values of the state couplings involve just the field angles $\delta\phi_{\mathcal{E}}$ and $\delta\theta_{\pm}$.

The above expression demonstrates that $\langle O(\tau)\rangle$ is potentially complicated for general state couplings and distribution functions and that it is difficult to extract all of the information encoded in the oscillatory term. A clearer analysis of the oscillatory term is obtained by performing a Fourier cosine transformation

$$\begin{aligned}
&\langle O(\nu)\rangle \\
&= \frac{2}{\pi}\int_0^\infty\langle O(\tau)\rangle\cos\nu\tau\,d\tau \\
&= \langle|\mathcal{T}_{--}|^2\rangle\int_{-\infty}^{\infty}L(\nu,\delta\omega'_-,\gamma^p_{-0})F_-(\delta\omega'_-,\mu_-,\sigma_-)d\delta\omega'_- \\
&\quad+\langle|\mathcal{T}_{-+}|^2\rangle\int_{-\infty}^{\infty}L(\nu,\delta\omega'_+,\gamma^p_{+0})F_+(\delta\omega'_+,\mu_+,\sigma_+)d\delta\omega'_+ \\
&\quad-\langle|\mathcal{T}_{--}|^2|\mathcal{T}_{-+}|^2\rangle\int_{-\infty}^{\infty}\frac{1}{2}L(\nu,\delta\omega'_{+-},\gamma^p_{+-}) \\
&\quad\times F_{+-}\left(\frac{1}{2}\delta\omega'_{+-},\mu_{+-},\sigma_{+-}\right)d\delta\omega'_{+-},
\end{aligned} \tag{50}$$

where $L(\nu,x,\gamma) = \frac{1}{\pi}\left(\frac{\gamma}{\gamma^2+(\nu-x)^2} + \frac{\gamma}{\gamma^2+(\nu+x)^2}\right)$ is a sum of Lorentzian distributions. Consequently, it is clear that $\langle O(\nu)\rangle$ is comprised of a collection of lines at $\nu = \pm\mu_-, \pm\mu_+, \pm\mu_{+-}$, which have composite line shapes of L and the distribution functions of frequency shifts. The Fourier analysis of the oscillatory term therefore provides the frequency shifts, the state couplings as well as information about the distributions of the field parameters from the locations, intensities, and shapes of the lines. This additional information encoded in the line shapes can be used to infer details about the statistics of the local environment of the spin, a notion which (through a different approach) forms the basis of the recent proposals of decoherence imaging.[19–22]

The distribution function f of the field parameters $\mathcal{R}$ and $\mathcal{R}'$ can be itself constructed from the distributions of the electric-strain $\mathcal{E}_\perp$ and magnetic $\mathcal{B}_z$ field components. Let the distributions of the electric-strain and magnetic field components be ϵ and β, respectively, then[71]

$$\begin{aligned}
f(\mathcal{R}/\hbar,\mu_{\mathcal{R}},\sigma_{\mathcal{R}}) &= \frac{d}{d\mathcal{R}}\int_{\mathcal{R}\geqslant\sqrt{\mathcal{B}_z^2+\mathcal{E}_\perp^2}}\epsilon\left(\frac{\mathcal{E}_\perp}{\hbar},\mu_{\mathcal{E}},\sigma_{\mathcal{E}}\right) \\
&\quad\times\beta\left(\frac{\mathcal{B}_z}{\hbar},\mu_{\mathcal{B}},\sigma_{\mathcal{B}}\right)d\frac{\mathcal{E}_\perp}{\hbar}d\frac{\mathcal{B}_z}{\hbar}, \\
f(\mathcal{R}'/\hbar,\mu_{\mathcal{R}'},\sigma_{\mathcal{R}'}) &= \frac{d}{d\mathcal{R}'}\int_{\mathcal{R}'\geqslant\sqrt{\mathcal{B}_z^2+\mathcal{E}_\perp^2}}\epsilon\left(\frac{\mathcal{E}_\perp}{\hbar},\mu'_{\mathcal{E}},\sigma_{\mathcal{E}}\right) \\
&\quad\times\beta\left(\frac{\mathcal{B}_z}{\hbar},\mu'_{\mathcal{B}},\sigma_{\mathcal{B}}\right)d\frac{\mathcal{E}_\perp}{\hbar}d\frac{\mathcal{B}_z}{\hbar},
\end{aligned} \tag{51}$$

where it has been assumed that the variances of the electric-strain and magnetic field components are independent of their mean values.

The above construction can be demonstrated using the simple case where the variance of the nonaxial electric-strain field $\sigma_{\mathcal{E}}$ is negligible compared to the variance of the axial magnetic field $\sigma_{\mathcal{B}}$ and the mean values of the field components $\mu_{\mathcal{E}}$ and $\mu_{\mathcal{B}}$. Due to the dominance of paramagnetic impurities over electric impurities in diamond,[5,72] this simple case is applicable to most applications of the ground-state spin. Modeling the electric-strain field distribution $\epsilon = \delta(\mathcal{E}_\perp/\hbar - \mu_{\mathcal{E}})$ by a delta function and the magnetic field distribution $\beta = \mathcal{N}(\mathcal{B}_z/\hbar,\mu_{\mathcal{B}},\sigma_{\mathcal{B}})$ by a normal distribution $\mathcal{N}(x,\mu,\sigma) = e^{-\frac{(x-\mu)^2}{2\sigma^2}}/\sqrt{2\pi\sigma^2}$, the distribution function of $\mathcal{R}$ is

$$\begin{aligned}
&f(\mathcal{R}/\hbar,\mu_{\mathcal{R}},\sigma_{\mathcal{R}}) \\
&= N_{\mathcal{R}}(\mu,\sigma)\begin{cases}0, & u<1\\ \frac{\sqrt{u^2-1}}{u}[\mathcal{N}(\sqrt{u^2-1},\mu,\sigma) & \\ \quad+\mathcal{N}(-\sqrt{u^2-1},\mu,\sigma)], & u\geqslant 1\end{cases}
\end{aligned} \tag{52}$$

where $u = \mathcal{R}/\hbar\mu_{\mathcal{E}}$, $\mu = \mu_{\mathcal{B}}/\mu_{\mathcal{E}}$, $\sigma = \sigma_{\mathcal{B}}/\mu_{\mathcal{E}}$, and $N_{\mathcal{R}}(\mu,\sigma)$ is a normalization constant. Note that an analogous expression can be obtained for $\mathcal{R}'$ by substituting the respective mean values and variances of the field components.

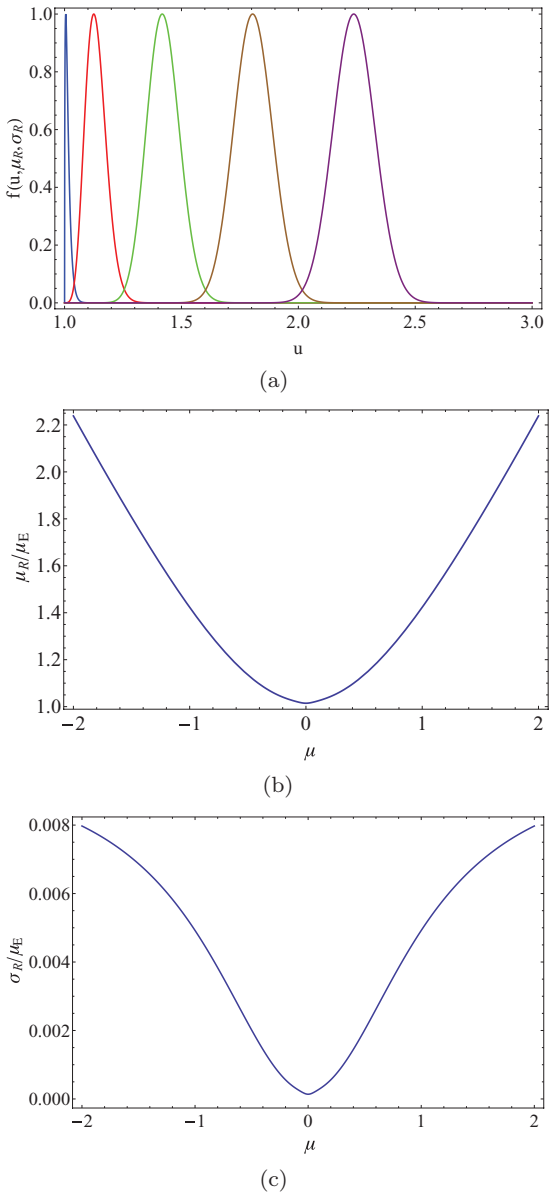

FIG. 7. (Color online) The distribution $f(\mathcal{R}/\hbar,\mu_{\mathcal{R}},\sigma_{\mathcal{R}})$ constructed for the simple case where the distribution of the nonaxial electric-strain component has negligible variance compared to the variance of the axial magnetic field component $\sigma_{\mathcal{B}}$ and the mean values of the field components $\mu_{\mathcal{E}}$ and $\mu_{\mathcal{B}}$. (a) Plots of the distribution as a function of $u = \mathcal{R}/\hbar\mu_{\mathcal{E}}$ for $\mu = \mu_{\mathcal{B}}/\mu_{\mathcal{E}} = 0,1/2,1,3/2,2$ (in sequential order left to right) and the same variance $\sigma = \sigma_{\mathcal{B}}/\mu_{\mathcal{E}} = 0.1$. (b) and (c) are plots of the mean $\mu_{\mathcal{R}}/\mu_{\mathcal{E}}$ and variance $\sigma_{\mathcal{R}}/\mu_{\mathcal{E}}$ of the distribution as a function of the axial magnetic field mean μ given $\sigma = 0.1$.

Figure 7(a) contains plots of the above distribution of $\mathcal{R}$ for the relative magnetic field variance $\sigma = 0.1$ and for different relative axial magnetic field mean values μ. As demonstrated by Figs. 7(b) and 7(c), the mean of the distribution of $\mathcal{R}$ varies as $\mu_{\mathcal{R}}/\mu_{\mathcal{E}} = \sqrt{\mu^2+1}$, which would be expected from the relationship $\mathcal{R} = \sqrt{\mathcal{B}_z^2 + \mathcal{E}_\perp^2}$, and that the variance $\sigma_{\mathcal{R}}/\mu_{\mathcal{E}}$ depends sensitively on the relative axial magnetic field mean μ, except for $\mu \gg 1$, where the variance becomes approximately independent of μ.

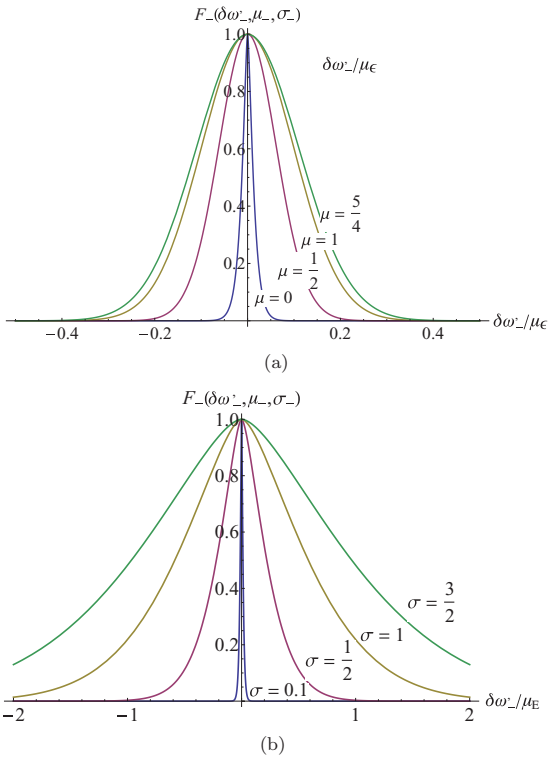

FIG. 8. (Color online) Plots of the distribution $F_-(\delta\omega'_-,\mu_-,\sigma_-)$ that describes the contribution of static field inhomogeneities to the shape of the line that occurs in the FID experiment that is used to measure the T_2^* time of the ground-state spin. (a) The distribution for different values of $\mu = \mu_{\mathcal{B}}/\mu_{\mathcal{E}} = 0,1/2,1,5/4$ and $\sigma = \sigma_{\mathcal{B}}/\mu_{\mathcal{E}} = 0.1$. (b) The distribution for different values of $\sigma = 0.1,1/2,1,3/2$ and $\mu = 0$. Note that each distribution has been normalized such that its maximum is 1.

Consider a FID experiment where the static fields do not differ in the period of free evolution. Such FID experiments are typically used to measure the T_2^* time of the ground-state spin via the width of the single line that occurs at $\delta\omega'_- = 0$ in the Fourier spectrum of the oscillatory term. Noting that for such an experiment $\langle|\mathcal{T}_{-+}|^2\rangle = \langle|\mathcal{T}_{--}|^2\mathcal{T}_{-+}|^2\rangle = 0$, $\mu_{\mathcal{R}} = \mu_{\mathcal{R}'}$, $\sigma_{\mathcal{R}} = \sigma_{\mathcal{R}'}$, and $\delta\mathcal{D} = 0$, the expression for the Fourier spectrum (50) simplifies to

$$\langle O(\nu)\rangle = \int_{-\infty}^{\infty} L\left(\nu,\delta\omega'_-,\gamma_{-0}^p\right) F_-(\delta\omega'_-,\mu_-,\sigma_-)\,d\delta\omega'_-, \quad (53)$$

where

$$F_-(\delta\omega'_-,\mu_-,\sigma_-) = \int_0^{\infty} f(\mathcal{R}/\hbar,\mu_{\mathcal{R}},\sigma_{\mathcal{R}}) \times f(\delta\omega'_- + \mathcal{R}/\hbar,\mu_{\mathcal{R}},\sigma_{\mathcal{R}})\,d\mathcal{R}/\hbar, \quad (54)$$

and assuming the simple case of negligible electric-strain field variance, the distribution f is given by (52). Since the line shape is a composition of L and F_-, the width of the line, and thus the T_2^* time of the spin, will depend on both the dephasing rate γ_{-0}^p and the electric-strain and magnetic field distribution parameters that form F_-.

The distribution F_- is plotted in Fig. 8 for different values of the relative axial magnetic field mean μ and variance σ. The plots clearly demonstrate that the width of the F_- distribution

is highly dependent on μ, such that it increases significantly for small increases in μ until $\mu \sim 1$. In the limit $\mu \gg 1$, it can be seen that the distribution has reached its maximum width and is very similar to a normal distribution. This is consistent with the distribution of $\mathcal{R}$ being dominated by the distribution of $\mathcal{B}_z$ when the mean axial magnetic field is much larger than the mean nonaxial electric-strain field. Hence, it can be concluded that due to the dominance of magnetic inhomogeneities, the contribution to the spin's T_2^* time from statistical inhomogeneities in the static fields is dramatically reduced for field configurations where $\mu = \mu_{\mathcal{B}}/\mu_{\mathcal{E}} < 1$. This conclusion is consistent with the observations of the recent electric field sensing demonstration[12] and has significant implications for the spin's other sensing and QIP applications.

VII. SPIN RELAXATION AND DEPHASING

As noted in Sec. III, the ground-state spin interacts with time-dependent incoherent electric and magnetic fields and crystal vibrations, which introduce the spin relaxation γ_{ij}^r and dephasing γ_{ij}^p rates into the evolution of the spin. The incoherent electric and magnetic fields arise from the thermal radiation field and fluctuating magnetic and electric impurities and the crystal vibrations arise from the thermal motion of the crystal nuclei. Typical of spin systems, spontaneous radiative emission and contributions from the thermal field are negligible and can be safely ignored.[68] As identified in Sec. II, the spin's interaction with electric fields is much smaller than its interactions with magnetic and strain fields. Consequently, the relaxation and dephasing rates are expected to be well described by just the spin's interactions with magnetic impurities and lattice vibrations. The contributions to relaxation and dephasing arising from interactions with magnetic impurities, including their dependence on the static magnetic field, has been studied in some detail for NV spins in both type-Ib and type-IIa diamond.[3,72–80] The additional influence of electric-strain fields on these interactions has not yet been studied and this will be the subject of future work. In this section, the contributions to relaxation and dephasing arising from the spin's interaction with lattice vibrations will be theoretically developed.

The linear interaction of the spin with the vibrations of the crystal is described by the potential[62]

$$\hat{V}_{\text{vib}} = \sum_i \sum_{u,q} \frac{\partial \hat{V}_{Ne}(\vec{r}_i, \vec{R})}{\partial Q_{u,E,q}}\bigg|_{\vec{R}_0} \sqrt{\frac{\hbar}{2\omega_{u,E}}} (\hat{b}_{u,E,q} + \hat{b}^\dagger_{u,E,q}), \tag{55}$$

where as for the interaction of the spin with a static strain field, $Q_{u,E,q}$ is defined as the uth mass-weighted normal displacement coordinate of symmetry (E,q) that corresponds to an eigenmode of the ground triplet with frequency $\omega_{u,E}$ in the harmonic approximation, $\vec{R}_0$ are the ground-state equilibrium coordinates, and $\hat{b}_{u,E,q}$ and $\hat{b}^\dagger_{u,E,q}$ are the vibration annihilation and creation operators, respectively. Constructed in an analogous fashion to the matrix representation of the spin's interaction with the strain field $\hat{V}_{\text{str}}$, the matrix representation of $\hat{V}_{\text{vib}}$ in the spin basis $\{|0\rangle, |-\rangle, |+\rangle\}$ is

$$\hat{V}_{\text{vib}} = \sum_u q_u \sqrt{\frac{\hbar}{2\omega_{u,E}}} \left[\begin{pmatrix} 0 & \frac{\chi}{\sqrt{2}}\left(e^{i\frac{\phi_{\mathcal{E}}}{2}} s_{\frac{\theta}{2}} - e^{-i\frac{\phi_{\mathcal{E}}}{2}} c_{\frac{\theta}{2}}\right) & \frac{\chi}{\sqrt{2}}\left(e^{i\frac{\phi_{\mathcal{E}}}{2}} c_{\frac{\theta}{2}} + e^{-i\frac{\phi_{\mathcal{E}}}{2}} s_{\frac{\theta}{2}}\right) \\ \frac{\chi}{\sqrt{2}}\left(e^{-i\frac{\phi_{\mathcal{E}}}{2}} s_{\frac{\theta}{2}} - e^{i\frac{\phi_{\mathcal{E}}}{2}} c_{\frac{\theta}{2}}\right) & -s_\theta c_{\phi_{\mathcal{E}}} & -c_\theta c_{\phi_{\mathcal{E}}} \\ \frac{\chi}{\sqrt{2}}\left(e^{-i\frac{\phi_{\mathcal{E}}}{2}} c_{\frac{\theta}{2}} + e^{i\frac{\phi_{\mathcal{E}}}{2}} s_{\frac{\theta}{2}}\right) & -c_\theta c_{\phi_{\mathcal{E}}} & s_\theta c_{\phi_{\mathcal{E}}} \end{pmatrix} \mathcal{Q}_{u,E,x} \right.$$
$$\left. + \begin{pmatrix} 0 & \frac{i\chi}{\sqrt{2}}\left(e^{i\frac{\phi_{\mathcal{E}}}{2}} s_{\frac{\theta}{2}} + e^{-i\frac{\phi_{\mathcal{E}}}{2}} c_{\frac{\theta}{2}}\right) & \frac{i\chi}{\sqrt{2}}\left(e^{i\frac{\phi_{\mathcal{E}}}{2}} c_{\frac{\theta}{2}} - e^{-i\frac{\phi_{\mathcal{E}}}{2}} s_{\frac{\theta}{2}}\right) \\ \frac{-i\chi}{\sqrt{2}}\left(e^{-i\frac{\phi_{\mathcal{E}}}{2}} s_{\frac{\theta}{2}} + e^{i\frac{\phi_{\mathcal{E}}}{2}} c_{\frac{\theta}{2}}\right) & -s_\theta s_{\phi_{\mathcal{E}}} & -c_\theta s_{\phi_{\mathcal{E}}} \\ \frac{-i\chi}{\sqrt{2}}\left(e^{-i\frac{\phi_{\mathcal{E}}}{2}} c_{\frac{\theta}{2}} - e^{i\frac{\phi_{\mathcal{E}}}{2}} s_{\frac{\theta}{2}}\right) & -c_\theta s_{\phi_{\mathcal{E}}} & s_\theta s_{\phi_{\mathcal{E}}} \end{pmatrix} \mathcal{Q}_{u,E,y} \right], \tag{56}$$

where $q_u = -\sqrt{2} s_{2,5} \langle a_1 || \partial \hat{V}_{Ne}/\partial Q_{u,E}|_{\vec{R}_0} || e\rangle$, $\chi = -\frac{\sqrt{2}s_{2,6}+s_{1,8}}{2\sqrt{2}s_{2,5}}$, and $\mathcal{Q}_{u,E,q} = \hat{b}_{u,E,q} + \hat{b}^\dagger_{u,E,q}$.

Applying time-dependent perturbation theory, the above matrix representation can be used to derive the first-order spin-lattice transition rates, which will contribute to both the relaxation and dephasing rates of the spin. The first-order spin-lattice transition rates are

$$W^{\text{vib}(1)}_{\pm\to 0} = \frac{\pi \chi^2}{\hbar} \frac{\overline{q^2}(\omega_\pm)\rho_E(\omega_\pm)}{\omega_\pm} [n_T(\omega_\pm) + 1],$$

$$W^{\text{vib}(1)}_{0\to\pm} = \frac{\pi \chi^2}{\hbar} \frac{\overline{q^2}(\omega_\pm)\rho_E(\omega_\pm)}{\omega_\pm} n_T(\omega_\pm),$$

$$W^{\text{vib}(1)}_{+\to -} = \frac{\pi}{\hbar} \cos^2\theta \frac{\overline{q^2}(\omega_{+-})\rho_E(\omega_{+-})}{\omega_{+-}} [n_T(\omega_{+-}) + 1],$$

$$W^{\text{vib}(1)}_{-\to +} = \frac{\pi}{\hbar} \cos^2\theta \frac{\overline{q^2}(\omega_{+-})\rho_E(\omega_{+-})}{\omega_{+-}} n_T(\omega_{+-}), \tag{57}$$

where $\overline{q^2}(\omega)$ is the average of q_u^2 over all E symmetric vibrations of frequency ω, $\rho_E(\omega)$ is the density of E symmetric vibrations at frequency ω, and $n_T(\omega) = 1/(e^{\hbar\omega/k_B T} - 1)$ is the mean occupation number of thermal vibrations given by the Bose-Einstein factor.

The NV transition frequencies $\omega_\pm$ and ω_{+-} occupy the very low frequency end of the vibrational frequencies of diamond, which range from zero to the Debye frequency of diamond $\omega_D = 38.76$ THz.[81] In the low-frequency limit,

the long-wavelength acoustic modes of the lattice have the well-known Debye density $\rho_E(\omega) \approx \rho_a \omega^2$, where ρ_a is a constant related to the acoustic velocity in diamond, and the electron-vibration interaction for the nonlocal acoustic modes has the approximate form $\overline{q^2}(\omega) \approx \omega \overline{q_a^2}$, where $\overline{q_a^2}$ is a constant.[82] Additionally, for temperatures $k_B T \gg \hbar\omega_\pm$, $\hbar\omega_{+-}$, the thermal occupations of the vibrational modes with frequencies corresponding to the NV transition frequencies can be approximated by $n_T(\omega) \approx k_B T/\hbar\omega$.[62] The first-order transition rates for temperatures $k_B T \gg \hbar\omega_\pm, \hbar\omega_{+-}$ are thus approximately linear in T:

$$\begin{aligned} W^{\mathrm{vib}(1)}_{\pm\to 0} &\approx W^{\mathrm{vib}(1)}_{0\to\pm} \approx \mathcal{A}_a \chi^2 \omega_\pm^2 T, \\ W^{\mathrm{vib}(1)}_{+\to -} &\approx W^{\mathrm{vib}(1)}_{-\to +} \approx \mathcal{A}_a \cos^2\theta \omega_{+-}^2 T, \end{aligned} \tag{58}$$

where $\mathcal{A}_a = \pi k_B \rho_a \overline{q_a^2}/\hbar^2$. Noting that for an axially aligned magnetic field, $\omega_{+-}^2 \cos^2\theta = 4\mathcal{B}_z^2$ and $\omega_\pm = (\mathcal{D} \pm \mathcal{R})^2$, it is clear that the first-order transitions between different spin states depend differently on the field parameters.

Since the electron-vibration interaction $\overline{q^2}(\omega)$ and the density of vibrational modes $\rho_E(\omega)$ increase at higher vibrational frequencies, the first-order transitions will only be the dominant spin-lattice mechanisms at low temperatures, where there are only appreciable occupations of the low-frequency vibrational modes. At higher temperatures, the occupation of the more numerous and strongly interacting higher-frequency modes ensures that elastic and inelastic Raman scattering of vibrations will become the dominant spin-lattice mechanisms.[62] The inelastic scatterings will contribute to both relaxation and dephasing, whereas the elastic scatterings will contribute to just dephasing. Note that as the two-vibration absorption/emission transitions involve vibrations of even lower frequencies than the first-order transitions, they will be negligible at all temperatures. Applying second-order time-dependent perturbation theory using (55) and expecting the most significant contributions to be from vibrational modes with frequencies $\omega \gg \omega_\pm$, ω_{+-}, the elastic and inelastic Raman scattering rates are approximately

$$\begin{aligned} W^{\mathrm{vib}(2)}_{\pm\to 0} &\approx W^{\mathrm{vib}(2)}_{0\to\pm} \approx W^{\mathrm{vib}(2)}_{\pm\to\mp} \approx \frac{1}{2} W^{\mathrm{vib}(2)}_{0\to 0} \\ &\approx \frac{\pi\chi^2}{\hbar^2} \int_0^{\omega_D} \frac{\overline{q^2}^2(\omega)\rho_E^2(\omega)}{\omega^4} n_T(\omega)[n_T(\omega)+1] d\omega, \\ W^{\mathrm{vib}(2)}_{\pm\to\pm} &\approx \frac{\pi}{\hbar^2}[1 + \chi^2(1 \pm \sin\theta\cos 3\phi_\mathcal{E}) + \chi^4] \\ &\quad \times \int_0^{\omega_D} \frac{\overline{q^2}^2(\omega)\rho_E^2(\omega)}{\omega^4} n_T(\omega)[n_T(\omega)+1] d\omega. \end{aligned} \tag{59}$$

Note that the above transition rates include contributions from all Raman-type transitions that involve the creation and annihilation of one vibration and whose intermediate states are restricted to the spin states of the ground triplet state.

The dependence of the elastic scattering rates of the $|\pm\rangle$ spin states on the static field angles is particularly interesting. Figure 9 contains polar plots of the dimensionless scattering parameter $[1 + \chi^2(1 \pm \sin\theta\cos 3\phi_\mathcal{E}) + \chi^4]$ as a function of the θ and $\phi_\mathcal{E}$ field angles for different values of χ. As can be seen, for $|\chi| > 0$, the elastic scattering rates are minimum at $\phi_\mathcal{E} = 0, \frac{2\pi}{3}, \frac{4\pi}{3}$, mimicking the structural symmetry of the defect center. Hence, it appears possible for the orientation of the nonaxial electric-strain field to be tuned so that the elastic scattering rates are minimized or maximized with the difference in the minimum and maximum rates $2\chi^2$ determined by the ratio of spin coupling coefficients χ. Note that χ is currently unknown.

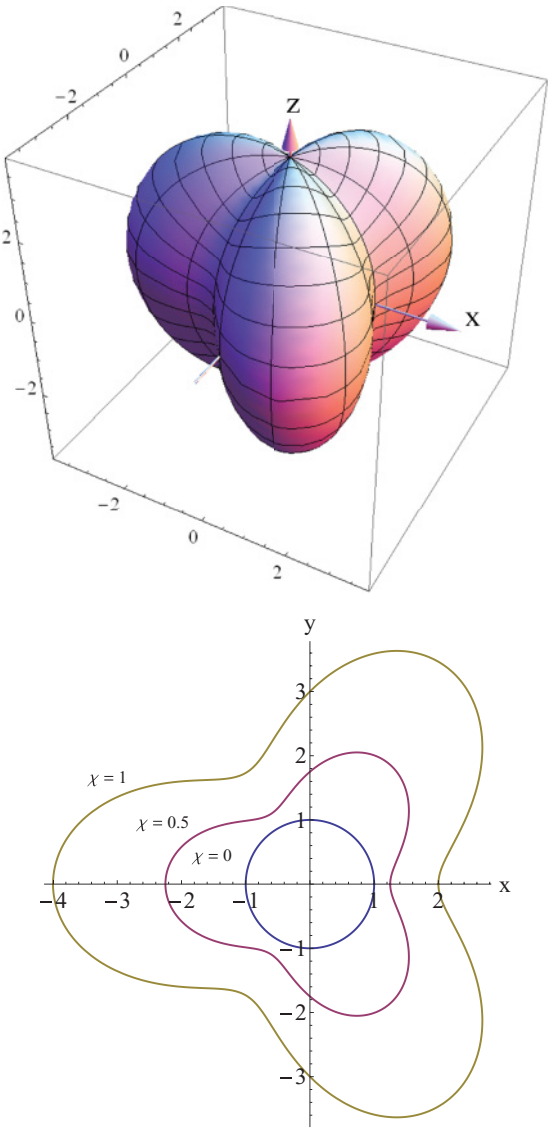

FIG. 9. (Color online) Plots of the dimensionless elastic vibration scattering parameter $[1 + \chi^2(1 - \sin\theta\cos 3\phi_\mathcal{E}) + \chi^4]$ as (a) a function of the azimuthal $0 \leqslant \phi_\mathcal{E} \leqslant 2\pi$ and polar $0 \leqslant \theta \leqslant \pi$ angles for $\chi = 1$; and (b) as a function of $\phi_\mathcal{E}$ for $\theta = \frac{\pi}{2}$ and different values of χ as indicated. Coordinate axes are provided for reference to Fig. 1 where the field angles $\phi_\mathcal{E}$ and θ are defined.

Considering temperatures not so high that optical modes are appreciably occupied in thermal equilibrium, there will be two distinct contributions to the integrals in the Raman scattering rates. The first will be from the acoustic modes which have electron-vibration interaction $\overline{q^2}(\omega) \approx \omega \overline{q_a^2}$ and mode density $\rho_E(\omega) \approx \rho_a \omega^2$. The second will be from the strongly interacting local modes of the NV center, which have frequencies $\omega_l \sim 65$ meV.[83] The contribution from the local modes can be represented by the electron-vibration

interaction $\overline{q^2}(\omega_l) \approx \overline{q_l^2}$ and a sharp peak in the density of modes centered at $\rho_E(\omega_l) = \rho_l$ with width σ_l. Given the separable contributions, the integrals can be evaluated and the Raman scattering rates reduce to

$$\begin{aligned} W^{\mathrm{vib}(2)}_{\pm\to 0} &\approx W^{\mathrm{vib}(2)}_{0\to\pm} \approx W^{\mathrm{vib}(2)}_{\pm\to\mp} \approx \frac{1}{2} W^{\mathrm{vib}(2)}_{0\to 0} \\ &\approx \chi^2 \left[\mathcal{A}_l^2 n_T(\omega_l)[n_T(\omega_l)+1] + \mathcal{A}_a^2 \frac{4\pi^3 k_B^3}{15\hbar^3} T^5 \right], \\ W^{\mathrm{vib}(2)}_{\pm\to\pm} &\approx [1 + \chi^2(1 \pm \sin\theta \cos 3\phi_{\mathcal{E}}) + \chi^4] \\ &\quad \times \left[\mathcal{A}_l^2 n_T(\omega_l)[n_T(\omega_l)+1] + \mathcal{A}_a^2 \frac{4\pi^3 k_B^3}{15\hbar^3} T^5 \right], \end{aligned} \tag{60}$$

where $\mathcal{A}_l^2 = \pi \overline{q_l^2}^2 \rho_l^2 \sigma_l^2 / \hbar^2 \omega_l^4$. Note that the integral over the acoustic modes was evaluated in the limit $\omega_D \to \infty$ in order to obtain the simple T^5 factor.[62,84,85] Given the temperatures being considered, for which high-frequency optical modes are not appreciably occupied, this extension of the integral is expected to be inconsequential. Hence, the Raman scattering rates depend on temperature in two distinct ways due to the distinct contributions of a few strongly interacting local modes and many weakly interacting nonlocal acoustic modes.

Combining the magnetic (W^B) and spin-lattice ($W^{\mathrm{vib}(1)}$ and $W^{\mathrm{vib}(2)}$) contributions, the relaxation and dephasing rates of the ground-state spin are

$$\begin{aligned} \gamma^r_{\pm 0} &= W^B_{\pm\to 0} + W^{\mathrm{vib}(1)}_{\pm\to 0} + W^{\mathrm{vib}(2)}_{\pm\to 0}, \\ \gamma^r_{0\pm} &= W^B_{0\to\pm} + W^{\mathrm{vib}(1)}_{0\to\pm} + W^{\mathrm{vib}(2)}_{0\to\pm}, \\ \gamma^r_{\pm\mp} &= W^B_{\pm\to\mp} + W^{\mathrm{vib}(1)}_{\pm\to\mp} + W^{\mathrm{vib}(2)}_{\pm\to\mp}, \\ \gamma^p_{\pm 0} &= \tfrac{1}{2}(\gamma^r_{\pm 0} + \gamma^r_{0\pm}) + W^B_{0\to 0} + W^B_{\pm\to\pm} + W^{\mathrm{vib}(2)}_{0\to 0} + W^{\mathrm{vib}(2)}_{\pm\to\pm}, \\ \gamma^p_{+-} &= \tfrac{1}{2}(\gamma^r_{+-} + \gamma^r_{-+}) + W^B_{-\to -} + W^B_{+\to +} + W^{\mathrm{vib}(2)}_{-\to -} + W^{\mathrm{vib}(2)}_{+\to +}. \end{aligned} \tag{61}$$

As described elsewhere, the magnetic contributions are highly dependent on the static magnetic field,[74,75,78–80] but are essentially temperature independent for temperatures > 20 K, due to the impurity spins easily reaching equal Boltzmann populations of their spin sublevels at low temperatures.[73] The spin-lattice contributions are instead weakly dependent on the static fields, but have distinct functions of temperature that arise from different interactions with lattice vibrations.

For a simple ODMR experiment using the ω_- transition, the spin relaxation T_1 and dephasing T_2 times are defined by $1/T_1 = \gamma^r_{-0} + \gamma^r_{0-}$ and $1/T_2 = \gamma^p_{-0}$, which, using the above, are explicitly

$$\begin{aligned} \frac{1}{T_1} &\approx 2\Gamma_{B1} + 2\Gamma_{\mathrm{vib}1}\omega_-^2 T + 2\Gamma_{\mathrm{vib}2} n_T(\omega_l)[n_T(\omega_l)+1] \\ &\quad + 2\Gamma_{\mathrm{vib}3} T^5, \\ \frac{1}{T_2} &\approx \frac{1}{2T_1} + \Gamma_{B2} + \left[\frac{1}{\chi^2} + (3 - \sin\theta\cos 3\phi_{\mathcal{E}}) + \chi^2 \right] \\ &\quad \times [\Gamma_{\mathrm{vib}2} n_T(\omega_l)[n_T(\omega_l)+1] + \Gamma_{\mathrm{vib}3} T^5], \end{aligned}$$

where $\Gamma_{\mathrm{vib}1} = \chi^2 \mathcal{A}_a$, $\Gamma_{\mathrm{vib}2} = \chi^2 \mathcal{A}_l^2$, and $\Gamma_{\mathrm{vib}3} = 4\pi\chi^2 k_B^3 \mathcal{A}_a^2 / 15\hbar^3$ are constants that are independent of the static fields and temperature, and Γ_{B1} and Γ_{B2} are the magnetic contributions that are dependent on the static fields, but effectively temperature independent. An analogous expression can be simply derived for the ω_+ transition.

Noting that $n_T(\omega_l)[n_T(\omega_l)+1] \approx n_T(\omega_l)$ for $k_B T < \hbar\omega_l$, the contribution to $1/T_1$ from inelastic Raman scatterings of strongly interacting local modes has been experimentally observed.[86] Likewise, the T and T^5 contributions from the weakly interacting acoustic modes have also been observed.[73] The spin-lattice contribution to $1/T_1$ only depends on the static fields through the presence of ω_-^2 in the linear temperature term. This dependence on the static fields has not yet been observed, which is most likely due to the insignificance of the linear term at ambient temperatures and the fact that most previous measurements have been performed using NV ensembles, where resonant interactions between NV subensembles and between NV centers and P1 centers at magnetic fields around $\mathcal{B} \sim 0$, 0.96, 1.44, and 1.68 GHz,[74,75] will most likely have masked the relatively weak dependence of the linear term. The dephasing rate $1/T_2$ is dominated by the contributions from magnetic interactions with little observed temperature dependence in small static fields.[3] Since the magnetic contribution is governed by the impurity concentration,[76] it may be possible to observe the spin-lattice contribution in highly pure samples. It would indeed be interesting to observe the tuning of $1/T_2$ using an electric-strain field via the spin-lattice elastic scattering parameter $[1/\chi^2 + (3 - \sin\theta\cos 3\phi_{\mathcal{E}}) + \chi^2]$.

VIII. CONCLUSION

In this article, the theory of the ground-state spin is fully developed using the molecular orbital theory of the center in order to provide detailed explanations for the spin's fine and hyperfine structures and its interactions with electric, magnetic, and strain fields. The explanations allowed the correlation of the properties of the ground-state spin with the other properties of the center and provided explicit expressions for the key parameters of spin in terms of the center's MOs. As a consequence, this work has identified the critical parameters that need to be pursued by future experimental and *ab initio* studies. Given the detailed theoretical development presented in Secs. II and III, a general solution was subsequently obtained for the NV spin in any given electric-magnetic-strain field configuration, and the effects of the fields on the spin's evolution, relaxation, and inhomogeneous dephasing were examined. In particular, the control of the spin's susceptibility to inhomogeneities in the static fields and crystal vibrations was examined in detail. The analysis of the effects of inhomogeneous fields revealed the field configurations required to switch between different noise-dominated regimes. The analysis of the spin's interactions with crystal vibrations yielded observable effects that are consistent with previous observations and also the basis for future investigations into the potential tuning of the spin's dephasing rate. Hence, in its entirety, this work has provided essential theoretical tools for the precise control and modeling of this remarkable spin in its current and future quantum metrology and QIP applications.

ACKNOWLEDGMENTS

This work was supported by the Australian Research Council under the Discovery Project scheme (DP0986635 and DP0772931), the EU commission (ERC grant SQUTEC), Specific Targeted Research Project DIAMANT, and the integrated project SOLID. F.D. wishes to acknowledge the Baden-Wuerttemberg Stiftung-Internationale Spitzenforschung-II.

[1] G. Balasubramanian *et al.*, Nature (London) **455**, 648 (2008).
[2] J. R. Maze *et al.*, Nature (London) **455**, 644 (2008).
[3] J. M. Taylor, P. Cappellaro, L. Childress, L. Jiang, D. Budker, P. R. Hemmer, A. Yacoby, R. Walsworth, and M. D. Lukin, Nat. Phys. **4**, 810 (2008).
[4] C. L. Degen, Appl. Phys. Lett. **92**, 243111 (2008).
[5] G. Balasubramanian *et al.*, Nat. Mater. **8**, 383 (2009).
[6] S. Steinert, F. Dolde, P. Neumann, A. Aird, B. Naydenov, G. Balasubramanian, F. Jelezko, and J. Wrachtrup, Rev. Sci. Instrum. **81**, 043705 (2010).
[7] B. Naydenov, F. Dolde, L. T. Hall, C. Shin, H. Fedder, L. C. L. Hollenberg, F. Jelezko, and J. Wrachtrup, Phys. Rev. B **83**, 081201(R) (2011).
[8] L. P. McGuinness *et al.*, Nat. Nanotechnol. **6**, 358 (2011).
[9] C. A. Meriles, L. Jiang, G. Goldstein, J. S. Hodges, J. Maze, M. D. Lukin, and P. Cappellaro, J. Chem. Phys. **133**, 124105 (2010).
[10] G. de Lange, D. Riste, V. V. Dobrovitski, and R. Hanson, Phys. Rev. Lett. **106**, 080802 (2011).
[11] L.-S. Bouchard, V. M. Acosta, E. Bauch, and D. Budker, New J. Phys. **13**, 025017 (2011).
[12] F. Dolde *et al.*, Nat. Phys. **7**, 459 (2011).
[13] E. Togan, Y. Chu, A. S. Trifonov, L. Jiang, J. Maze, L. Childress, M. V. G. Dutt, A. S. Soerensen, P. R. Hemmer, A. S. Zibrov, and M. D. Lukin, Nature (London) **466**, 730 (2010).
[14] P. Neumann, N. Mizouchi, F. Rempp, P. Hemmer, H. Watanabe, S. Yamasaki, V. Jacques, T. Gaebel, F. Jelezko, and J. Wrachtrup, Science **320**, 1326 (2008).
[15] P. Neumann, R. Kolesov, B. Naydenov, J. Beck, F. Rempp, M. Steiner, V. Jacques, G. Balasubramanian, M. L. Markham, D. J. Twitchen, S. Pezzagna, J. Meijer, J. Twamley, F. Jelezko, and J. Wrachtrup, Nat. Phys. **6**, 249 (2010).
[16] P. Neumann, J. Beck, M. Steiner, F. Rempp, H. Fedder, P. R. Hemmer, J. Wrachtrup, and F. Jelezko, Science **329**, 542 (2010).
[17] G. Waldherr, J. Beck, M. Steiner, P. Neumann, A. Gali, Th. Frauenheim, F. Jelezko, and J. Wrachtrup, Phys. Rev. Lett. **106**, 157601 (2011).
[18] G. Waldherr, P. Neumann, S. F. Huelga, F. Jelezko, and J. Wrachtrup, Phys. Rev. Lett. **107**, 129901 (2011).
[19] J. H. Cole and L. C. L. Hollenberg, Nanotechnology **20**, 495401 (2009).
[20] L. T. Hall, J. H. Cole, C. D. Hill, and L. C. L. Hollenberg, Phys. Rev. Lett. **103**, 220802 (2009).
[21] L. T. Hall, C. D. Hill, J. H. Cole, and L. C. L. Hollenberg, Phys. Rev. B **82**, 045208 (2010).
[22] L. T. Hall, C. D. Hill, J. H. Cole, B. Stadler, F. Caruso, P. Mulvaney, J. Wrachtrup, and L. C. L. Hollenberg, Proc. Natl. Acad. Sci. USA **107**, 18777 (2010).
[23] J. Harrison, M. J. Sellars, and N. B. Manson, J. Lumin. **107**, 245 (2004).
[24] F. Jelezko and J. Wrachtrup, J. Phys.: Condens. Matter **16**, 1089 (2004).
[25] M. W. Doherty, N. B. Manson, P. Delaney, and L. C. L. Hollenberg, New J. Phys. **13**, 025019 (2011).
[26] L. J. Rogers *et al.*, New J. Phys. **11**, 063007 (2009).
[27] A. Batalov, V. Jacques, F. Kaiser, P. Siyushev, P. Neumann, L. J. Rogers, R. L. McMurtrie, N. B. Manson, F. Jelezko, and J. Wrachtrup, Phys. Rev. Lett. **102**, 195506 (2009).
[28] V. M. Acosta, E. Bauch, M. P. Ledbetter, A. Waxman, L.-S. Bouchard, and D. Budker, Phys. Rev. Lett. **104**, 070801 (2010).
[29] P. Neumann *et al.*, New J. Phys. **11**, 013017 (2009).
[30] G. D. Fuchs, V. V. Dobrovitski, R. Hanson, A. Batra, C. D. Weis, T. Schenkel, and D. D. Awschalom, Phys. Rev. Lett. **101**, 117601 (2008).
[31] N. R. S. Reddy, N. B. Manson, and E. R. Krausz, J. Lumin. **38**, 46 (1987).
[32] P. H. Tamarat *et al.*, New J. Phys. **10**, 045004 (2006).
[33] E. van Oort and M. Glasbeek, Chem. Phys. Lett. **168**, 529 (1990).
[34] L. du Preez, Ph.D. thesis, University of Witwatersand, 1965.
[35] L. J. Rogers, S. Armstrong, M. J. Sellars, and N. B. Manson, New J. Phys. **10**, 103024 (2008).
[36] F. Jelezko, T. Gaebel, I. Popa, A. Gruber, and J. Wrachtrup, Phys. Rev. Lett. **92**, 076401 (2004).
[37] L. Childress, M. V. G. Dutt, J. M. Taylor, A. S. Zibrov, F. Jelezko, J. Wrachtrup, P. R. Hemmer, and M. D. Lukin, Science **314**, 281 (2006).
[38] G. de Lange, Z. H. Wang, D. Riste, V. V. Dobrovitski, and R. Hanson, Science **330**, 60 (2010).
[39] C. A. Ryan, J. S. Hodges, and D. G. Cory, Phys. Rev. Lett. **105**, 200402 (2010).
[40] X-F. He, N. B. Manson, and P. T. H. Fisk, Phys. Rev. B **47**, 8809 (1993); **47**, 8816 (1993).
[41] J. P. Goss, R. Jones, S. J. Breuer, P. R. Briddon, and S. Oberg, Phys. Rev. Lett. **77**, 3041 (1996).
[42] M. Luszczek, R. Laskowski, and P. Horodecki, Phys. B (Amsterdam) **348**, 292 (2004).
[43] J. A. Larsson and P. Delaney, Phys. Rev. B **77**, 165201 (2008).
[44] C. Lin, Y. Wang, H. Chang, M. Hayashi, and S. H. Lin, J. Chem. Phys. **129**, 124714 (2008).
[45] Y. Ma, M. Rohlfing, and A. Gali, Phys. Rev. B **81**, 041204 (2010).
[46] F. M. Hossain, M. W. Doherty, H. F. Wilson, and L. C. L. Hollenberg, Phys. Rev. Lett. **101**, 226403 (2008).
[47] P. Delaney, J. C. Greer, and J. A. Larsson, Nano Lett. **10**, 610 (2010).
[48] A. Gali, E. Janzen, P. Deak, G. Kresse, and E. Kaxiras, Phys. Rev. Lett. **103**, 186404 (2009).
[49] A. Gali, M. Fyta, and E. Kaxiras, Phys. Rev. B **77**, 155206 (2008).
[50] J. H. N. Loubser and J. A. van Wyk, Rep. Prog. Phys. **41**, 1203 (1978).
[51] S. Felton, A. M. Edmonds, M. E. Newton, P. M. Martineau, D. Fisher, D. J. Twitchen, and J. M. Baker, Phys. Rev. B **79**, 075203 (2009).

[52]A. Lenef and S. C. Rand, Phys. Rev. B **53**, 13441 (1996).
[53]N. B. Manson, J. P. Harrison, and M. J. Sellars, Phys. Rev. B **74**, 104303 (2006).
[54]N. B. Manson, L. J. Rogers, M. W. Doherty, and L. C. L. Hollenberg, e-print arXiv:1011.2840.
[55]J. F. Cornwell, *Group Theory in Physics: An Introduction* (Academic, London, 1997).
[56]A. J. Stone, Proc. R. Soc. London, Ser. A **271**, 424 (1963).
[57]M. Steiner, P. Neumann, J. Beck, F. Jelezko, and J. Wrachtrup, Phys. Rev. B **81**, 035205 (2010).
[58]B. Smeltzer, J. McIntyre, and L. Childress, Phys. Rev. A **80**, 050302(R) (2009).
[59]P. Atkins and R. Friedman, *Molecular Quantum Mechanics* (Oxford Univeristy Press, New York, 2005).
[60]W. B. Mims, *The Linear Electric Field Effect in Paramagnetic Resonance* (Clarendon, Oxford, 1976).
[61]A. T. Collins, M. F. Thomaz, and M. I. B. Jorge, J. Phys. C: Solid State Phys. **16**, 2177 (1983).
[62]A. M. Stoneham, *Theory of Defects in Solids* (Oxford University Press, Oxford, 1975).
[63]D. B. Fitchen, *Physics of Color Centers* (Academic, New York, 1968).
[64]U. Volz and H. Schmoranzer, Phys. Scr., T **65**, 48 (1996).
[65]A. Abragam, *The Principles of Nuclear Magnetism* (Clarendon, Oxford, 1961).
[66]Thiago P. Alegre, C. Santori, G. Medeiros-Ribeiro, and R. G. Beausoleil, Phys. Rev. B **76**, 165205 (2007).
[67]R. Loudon, *The Quantum Theory of Light* (Oxford University Press, Oxford, 1973).
[68]J. A. Weil and J. R. Bolton, *Electron Paramagnetic Resonance: Elementary Theory and Practical Applications* (Wiley, New Jersey, 2007).
[69]A. Schweiger and G. Jeschke, *Principles of Pulse Electron Paramagnetic Resonance* (Oxford University Press, New York, 2001).
[70]V. M. Acosta, E. Bauch, M. P. Ledbetter, A. Waxman, L.-S. Bouchard, and D. Budker, Phys. Rev. Lett. **104**, 070801 (2010).
[71]H. Stark and J. W. Woods, *Probability, Random Processes, and Estimation Theory for Engineers* (Prentice Hall, New Jersey, 1994).
[72]N. Mizuochi, P. Neumann, F. Rempp, J. Beck, V. Jacques, P. Siyushev, K. Nakamura, D. J. Twitchen, H. Watanabe, S. Yamasaki, F. Jelezko, and J. Wrachtrup, Phys. Rev. B **80**, 041201(R) (2009).
[73]S. Takahashi, R. Hanson, J. van Tol, M. S. Sherwin, and D. D. Awschalom, Phys. Rev. Lett. **101**, 047601 (2008).
[74]E. van Oort and M. Glasbeek, Phys. Rev. B **40**, 6509 (1989).
[75]E. van Oort and M. Glasbeek, Appl. Magn. Reson. **2**, 291 (1991).
[76]T. A. Kennedy, F. T. Charnock, J. S. Colton, J. E. Butler, R. C. Linares, and P. J. Doering, Phys. Status Solidi B **233**, 416 (2002).
[77]T. A. Kennedy, J. S. Colton, J. E. Butler, R. C. Linares, and P. J. Doering, Appl. Phys. Lett. **83**, 4190 (2003).
[78]I. Popa, T. Gaebel, M. Domhan, C. Wittmann, F. Jelezko, and J. Wrachtrup, Phys. Rev. B **70**, 201203(R) (2004).
[79]R. Hanson, O. Gywat, and D. D. Awschalom, Phys. Rev. B **74**, 161203(R) (2006).
[80]J. R. Maze, J. M. Taylor, and M. D. Lukin, Phys. Rev. B **78**, 094303 (2008).
[81]R. Stedman, L. Almqvist, and G. Nilsson, Phys. Rev. **162**, 549 (1967).
[82]A. A. Maradudin, Solid State Phys. **18**, 273 (1966).
[83]G. Davies and M. F. Hamer, Proc. R. Soc. London, Ser. A **348**, 285 (1976).
[84]J. H. Van Vleck, Phys. Rev. **57**, 426 (1940).
[85]M. B. Walker, Can. J. Phys. **46**, 1347 (1968).
[86]D. A. Redman, S. Brown, R. H. Sands, and S. C. Rand, Phys. Rev. Lett. **67**, 3420 (1991).